Quantum confinement in low-dimensional Dirac materials

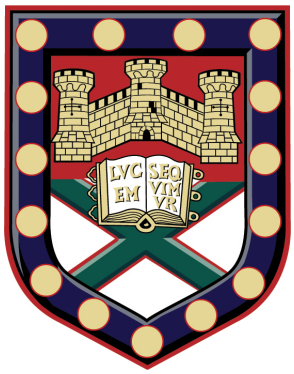

Charles Andrew Downing

School of Physics

University of Exeter

A thesis submitted for the degree of

Doctor of Philosophy in Physics

March 2015

Quantum confinement in low-dimensional Dirac materials

Submitted by Charles Andrew Downing to the University of Exeter as a thesis for the degree of Doctor of Philosophy in Physics.

March 2015

I certify that all material in this thesis which is not my own work has been identified and that no material has previously submitted and approved for the award of a degree by this or any other university.

Charles Andrew Downing

March 2015

The previous page was intentionally left blank.

The previous page was intentionally left with the message ‘The previous page was intentionally left blank’.

N. H. D. Bohr : What are you working on Mr. Dirac?

P. A. M. Dirac : I'm trying to take the square root of something.

- The 5th Solvay Conference, Brussels, 1927.

Abstract

This thesis is devoted to quantum confinement effects in low-dimensional Dirac materials. We propose a variety of schemes in which massless Dirac fermions, which are notoriously difficult to manipulate, can be trapped in a bound state. Primarily we appeal for the use of external electromagnetic fields. As a consequence of this endeavor, we find several interesting condensed matter analogues to effects from relativistic quantum mechanics, as well as entirely new effects and a possible novel state of matter.

For example, in our study of the effective Coulomb interaction in one dimension, we demonstrate how atomic collapse may arise in carbon nanotubes or graphene nanoribbons, and describe the critical importance of the size of the band gap. Meanwhile, inspired by groundbreaking experiments investigating the effects of strain, we propose how to confine the elusive charge carriers in so-called velocity barriers, which arise due to a spatially inhomogeneous Fermi velocity triggered by a strained lattice. We also present a new and beautiful quasi-exactly solvable model of quantum mechanics, showing the possibilities for confinement in magnetic quantum dots are not as stringent as previously thought. We also reveal that Klein tunnelling is not as pernicious as widely believed, as we show bound states can arise from purely electrostatic means at the Dirac point energy. Finally, we show from an analytical solution to the quasi-relativistic two-body problem, how an exotic same-particle paring can occur and speculate on its implications if found in the laboratory.

Contents

List of Figures

Acknowledgments

The way I see it, if you want the rainbow, you gotta put up with the rain.
- Dolly Parton

Firstly, I would like to thank my supervisor Prof. Mikhail Portnoi for his insight, enthusiasm and patience. Spasibo bol'shoye!

I would like express my gratitude to the School of Physics at the University of Exeter and the EPSRC (Engineering and Physical Sciences Research Council) for providing funding and resources, as well as the International Institute of Physics in Natal for their hospitality.

Many thanks to my friends and colleagues in the physics department: Arseny Alexeev, Robin Churchill, Chinna Devarapu, Chris Downs, Lachlan Marnham, Alex Pearce, Drew Pearce, Vasil Saroka, Tom Sturges and Claire Woollacott.

Finally, I would like to acknowledge my parents for parental support.

C. A. Downing

Exeter, United Kingdom

1th March 2015

But why, some say, study Dirac materials? Why choose this as our goal? And they may well ask, why climb the highest mountain? Why, 95 years ago, fly the Atlantic? Why does Rice play Texas? We choose to study Dirac materials. We choose to study Dirac materials in this decade and do the other things, not because they are easy, but because they are hard.

Chapter 1

Introduction

If you don’t know where you are going, any road will get you there.

- Lewis Carroll

At the start of 1928, Paul Adrien Maurice Dirac wrote down his eponymous relativistic wave equation for the electron [1]. From this brilliant result of human thought alone, Dirac was able to predict the existence of the positron and hence antimatter [2]. In 1933 he was duly decorated with a Nobel Prize, together with Erwin Schrödinger 'for the discovery of new productive forms of atomic theory'.

At the start of the new millennium, Russian-émigrés Andre Geim and Konstantin Novoselov started to conduct a series of playful experiments - so-called 'Friday night experiments' - at the University of Manchester. One such experiment was to simply play with Scotch tape and bulk graphite in the hope of being able to rip down to a few thin layers of graphite, from which a transistor could be made [3, 4]. In 2010, the pair were jointly awarded a Nobel Prize for 'groundbreaking experiments regarding the two-dimensional material graphene'.

These two historic scientific achievements are the foundations for the rise of Dirac materials: condensed matter systems which have excitations described by a Dirac-like equation [5, 6, 7]. Before Geim and Novoselov, Dirac physics was principally the domain of high energy physicists. Now the exciting fairground of quasi-relativistic phenomena, including *Zitterbewegung* [8] and Klein tunnelling [9], has been opened up to humble condensed matter scientists [10].

In 2005, it was shown by the group of Geim that many two-dimensional crystals (such as single layers of boron nitride, several dichalcogenides, and complex oxides) can be fabricated with the so-called mechanical exfoliation technique (pulling layers apart with sticky tape) [11]. However, the star among them was monolayer graphite: graphene. The list of graphene superlatives is remarkable, the material being: almost transparent (absorbing only 2.3% of incoming light intensity); the strongest material ever measured (more than 100 times stronger than the strongest steel); the stiffest known material (stiffer than diamond); the most stretchable crystal (up to 20% elastically); of record thermal conductivity (outperforming diamond); of record high current density at room temperature (106 times that of copper); completely impermeable (even helium cannot squeeze through) and of a record high intrinsic mobility (100 times more than in silicon). The distinctive honeycomb arrangement of carbon atoms in graphene is constructed from two tri-

angular sublattices which give rise to a degree of freedom analogous to spin (pseudospin) and arguably the most interesting property of graphene: excitations well described a massless Dirac-Weyl Hamiltonian around the K points, with a regime of validity up to around 500 meV. In some sense, this work fired the starting gun for researchers to uncover further low-dimensional Dirac materials. Below we outline a few examples.

Upon rolling up a sheet of graphene into a single-walled carbon nanotube, the boundary condition of periodicity around the circumference gives rise to a quantized transversal wavevector [12]. Depending on whether the wavevector is allowed or not, results in either a semiconducting or metallic nanotube, which can be described by a 1-D Dirac-like spectrum.

Transition metal dichalcogenides (TMDCs) - famous examples include molybdenum disulfide (MoS_2) and molybdenum diselenide ($MoSe_2$) - have been known for decades, however the realization of graphene and improvements in device fabrication have led to a resurgence in interest [13]. The class of materials belonging to the TMDC group is defined by the formula MX_2, where M is a group IV, V or VI transition metal element and X is a chalcogen (sulphur, selenide or tellurium). The materials are layered such that chalcogen atoms in two hexagonal planes are seperated by a metallic atomic plane (X-M-X). At the simplest level, they can be described by a massive Dirac Hamiltonian, with (unlike graphene) a non-negligible spin-orbit coupling term due to the presence of heavy metal atoms.

Three dimensional topological insulators (TIs) have a gapped spectrum in the bulk, but the surface states are described by a 2D Dirac equation [14, 15]. In this case, the Dirac nodes are protected by time-reversal symmetry [16, 17], rather than sublattice symmetry as found in graphene. The simplest class of such materials include bismuth selenide (Bi_2Se_3), bismuth telluride (Bi_2Te_3) and antimony telluride (Sb_2Te_3). There are also 2D TIs, such as mercury telluride/cadmium telluride (HgTe/CdTe) quantum wells [18] or indium arsenide/gallium antimonide (InAs/GaSb) quantum wells [19], where the chiral and helical edge states are described by a 1D Dirac equation. Finally, there are even 1D TIs, a historic example is polyacetylene [20], where the end states can be described by a Dirac Hamiltonian.

Other, perhaps more exotic, examples of where Dirac-like equations can appear in condensed matter physics include superfluid phases of ^{3}He [21] and high-temperature d-wave superconductors [22]. Furthermore, artificial honeycomb lattices can allow even more experimental control and scientifically rich explorations of Dirac physics, for example: cold atoms in an optical lattice [23]; microwaves in a lattice of dielectric resonators [24]; waves in photonic lattices [25]; plasmons in arrays of metallic nanoparticles [26, 27]; 'molecular graphene' or molecules assembled over a conventional 2D electron system by atomic manipulation [28] and a conventional 2D electron gas confined in semiconductor quantum wells via a superlattice created by nanopatterning [29].

The common thread running throughout this thesis is the difficulty in achieving bound states in Dirac materials [30]. A principal reason for this effect is due to the so-called Klein tunnelling [31], whereby a Dirac particle normally incident on an electrostatic barrier has a transmission probability tending towards one in the limit of a high barrier. This physically counterintuitive result has been dubbed Klein's paradox [32, 33, 34, 35]. In condensed matter physics, the resolution can be thought of as follows: normal incidence corresponds to a gapless band structure, thus there are always available states (either electron-like or hole-like) in which the propagating electron can tunnel through [9]. The mathematical reason is as follows: at normal incidence the transversal wavevector is zero, and so the two differential equations comprising the Dirac equation decouple. As there is only one solution to the remaining first order differential equations there is no room for a reflected solution, leaving just the transmitted solution.

This thesis will be organized into four chapters, with a chapter devoted to one-dimensional problems (Chapter 2) and a chapter to two-dimensional problems (Chapter 3) sandwiched in between this introduction Chapter 1 and a conclusion Chapter 4, where possible extension of this work are also discussed.

Chapter 2 is further divided into two sections. In the first of which, Sec. 2.1, we encounter a low-dimensional analogue of the famous 'fall-into the-center' problem at the heart of quantum mechanics, with the significant advantage that as it appears in a mesoscopic systems it should be within the experimentalists reach to see in the laboratory. This chapter is closed by Sec. 2.2, where we investigate confinement by so-called velocity

barriers, formed by a spatially inhomogeneous Fermi velocity.

Chapter 3 is split into four sections. Firstly, we consider bound states in both magnetic quantum dots and rings in Sec. 3.1. Secondly, we present a study of fully confined zero-energy states in electrostatic fields with (and without) the influence of a magnetic flux in Sec. 3.2. Thirdly, we further investigate zero-energy states, with a focus on their impact on scattering in Sec. 3.3. Finally in Sec. 3.4, we propose the existence of a novel quasiparticle composed of a bound pair, either electron-hole or even bielectron, which may form in gated graphene structures.

Chapter 2

One dimensional problems

The true delight is in the finding out rather than in the knowing.

- Isaac Asimov

2.1 Atomic collapse

We investigate the one-dimensional Coulomb potential with application to a class of quasi-relativistic systems, so-called Dirac-Weyl materials, described by matrix Hamiltonians. We obtain the exact solution of the shifted and truncated Coulomb problems, with the wavefunctions expressed in terms of special functions (namely Whittaker functions), whilst the energy spectrum must be determined via solutions to transcendental equations. Most notably, there are critical bandgaps below which certain low-lying quantum states are missing in a manifestation of atomic collapse.

2.1.1 Introduction

The Coulomb problem in quantum theory is a historic problem of theoretical physics [36]. Its solution, which can be written down analytically, is a cornerstone of quantum mechanics and gives tremendous insight into the hydrogen atom [37, 38, 39]. Moreover, its solution in reduced dimensions is also highly significant: experiments with electrons confined to a plane led to considerations of the Coulomb problem in two dimensions (2D) [40, 41, 42, 43], whilst the history of the one-dimensional (1D) Coulomb problem is long, interesting and sometimes controversial [44, 45, 46].

The analogous relativistic problem [47, 48, 49] as governed by Dirac's equation, is equally fascinating and likewise the problem has also been investigated in low dimensions, both in 2D [50, 51] and 1D [52, 53, 54]. The rise of Dirac materials [6], condensed matter systems with quasi-particles well-described by the Dirac equation, has led to revisits of Dirac-Kepler problems with Dirac-like matrix Hamiltonians. One example is the 2D relativistic solution and its application to graphene [55, 56], which has charge carriers described by a massless Dirac-Weyl equation. Graphene, a single atomic layer of carbon atoms in a honeycomb lattice [57], is the star of the Dirac materials; however, there are in fact a plethora of other materials such as topological insulators [14, 15], transition metal dichalcogenides [59], carbon nanotubes [60] and 3D Weyl semimetals [61], which provide physicists a new playground to investigate quasi-relativistic phenomena.

Here we look at the quasi-relativistic Coulomb problem in 1D at the level of a two-by-two Dirac-like matrix Hamiltonian. Our results should be useful in several areas for

various quasi-1D Dirac systems, most notably narrow-gap carbon nanotubes and graphene nanoribbons, for example: in the understanding of the energy spectra of donors and excitons, table-top experiments on atomic collapse, vacuum polarization effects, Sommerfeld factor and the suppression of van Hove singularities, Coulomb blockade and zero-bias anomalies, magnetoexcitons and so on. Besides, the intrinsic beauty of analytic results in quantum mechanics is almost always coupled with greater insight, as well as being sturdy platforms on which to test new numerical methods or perturbative schemes.

The low-energy spectrum of a typical 1D Dirac material can be described by a single-particle, single-valley matrix Hamiltonian

$$\hat{H}_1 = v_F \begin{pmatrix} 0 & \hat{p}_x - i\hbar\Delta \\ \hat{p}_x + i\hbar\Delta & 0 \end{pmatrix} + U(x) \tag{2.1}$$

where v_F is the Fermi velocity (which can be for example $v_F \approx c/300$ for carbon nanotubes or graphene nanoribbons), $2\hbar v_F|\Delta|$ is the bandgap and the momentum operator $\hat{p}_x$ acts along the axis of the effectively 1D system. The same Hamiltonian, Eq. (2.1), describes a 2D Weyl material, e.g. graphene or the surface of a topological insulator, subjected to a 1D potential $V(x)$ constant in the y-direction, in which case $\Delta \to k_y$ [62]. We assume $V(x)$ is sufficiently smooth on the atomic scale, such that inter-valley scattering can be neglected. We make the unitary transform $U = \frac{1}{\sqrt{2}}\left(\begin{smallmatrix} 1 & 1 \\ 1 & -1 \end{smallmatrix}\right)$ with Eq. (2.1) to construct a basis of symmetric and antisymmetric wavefunctions and obtain the following system of equations

$$\begin{pmatrix} \partial_x & -\Delta \\ \Delta & -\partial_x \end{pmatrix} \begin{pmatrix} \psi_1(x) \\ \psi_2(x) \end{pmatrix} = i(\varepsilon - V(x)) \begin{pmatrix} \psi_1(x) \\ \psi_2(x) \end{pmatrix}. \tag{2.2}$$

where we have scaled the eigenvalue $\varepsilon = E/\hbar v_F$ and potential energy $V(x) = U(x)/\hbar v_F$.

In what follows we investigate the quasi-1D Coulomb potential with two different modifications, the so-called 'shifted' and 'truncated' Coulomb problems. Both modifications introduce a regularization scheme at the origin, so as to avoid problematic boundary conditions well known in the non-relativistic case [44] and more importantly to be more physically meaningful. A cut-off naturally arises in nanotubes and quantum wires due to the finite (albeit small) size of the quantum confined direction, which is related to the

radius of the wire [63]. The third main alteration to the Coulomb potential is the Ohno potential [64], but we omit a treatment of this case as it is only quasi-exactly solvable [65] in terms of confluent Heun functions [66].

For completeness, we note that exponentially decaying potentials, which are of a short-range nature, have also been considered in quasi-1D Dirac systems in various forms [67, 68, 69]. However, it is the pure Coulombic long-range interaction, decreasing like the inverse of separation, which is the subject of this work as it is well known that screening is suppressed in low-dimensional systems [70]. Indeed, in the case of 2D Dirac-Weyl systems like graphene screening does not alter the long range functional dependence of the Coulomb interaction beyond a slow, logarithmic correction [57, 58], whilst screening is further reduced in carbon nanotubes [60]. Additionally, in a similar framework to this work, transmission problems through periodic potentials [71] as well as linear [72] and smooth step potentials [73] have been treated.

Furthermore, it should be mentioned that the confinement of Dirac-like particles in one-dimensional potentials is the subject of considerable recent attention from the applied mathematics community [74, 75, 76, 77, 78]. Our results here, using two explicit toy models of non-integrable potentials, provide a complementary approach both more accessible to physicists and closer to experimental reality.

2.1.2 The shifted Coulomb problem

In this section we shall investigate the shifted 1D Coulomb potential plotted in Fig. 2.1 and explicitly given by

$$V_s(x) = \frac{-U_0}{a + |x|}, \tag{2.3}$$

where a is the shift length, and the dimensionless number $U_0 = \frac{e^2}{4\pi\epsilon}\frac{1}{\hbar c}\frac{c}{v_F}$ is an effective fine structure constant, which in the case of carbon nanotubes or graphene nanoribbons is $U_0 \approx \frac{300}{137}$.

Upon substitution of Eq. (2.3) into Eq. (2.2), the wavefunction component $\psi_1(x)$ in the region II ($x > 0$) satisfies a modified form of the confluent hypergeometric equation,

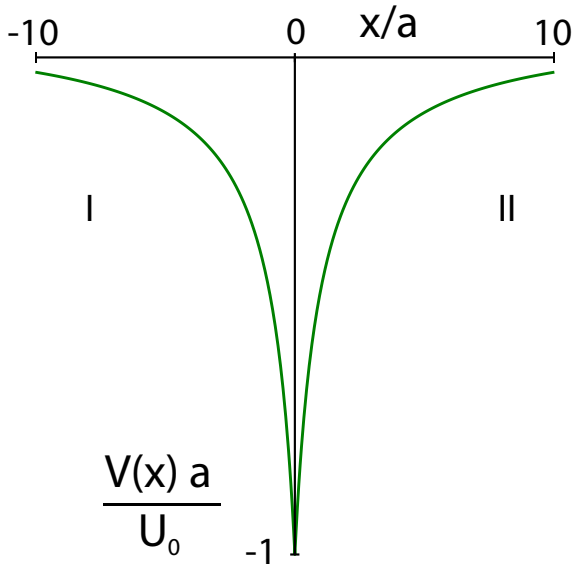

Figure 2.1: A plot of the shifted Coulomb potential, defined by Eq. (2.3).

called the Whittaker differential equation, in the variable $\xi = 2\kappa(a + x)$,

$$\frac{d^2}{d\xi^2}\psi_1(\xi) + \left(-\frac{1}{4} + \frac{\mu}{\xi} + \frac{1/4 - \nu^2}{\xi^2}\right)\psi_1(\xi) = 0, \tag{2.4}$$

where

$$\mu = \frac{\varepsilon U_0}{\kappa}, \quad \nu = iU_0 - \frac{1}{2}, \tag{2.5}$$

with $\kappa = \sqrt{\Delta^2 - \varepsilon^2} > 0$, as we consider bound states ($|\varepsilon| < |\Delta|$) only. An asymptotically convergent solution can be constructed, known as the Whittaker function of the second kind [79]

$$W_{\mu,\nu}(\xi) = \xi^{1/2+\nu} e^{-\xi/2} U\left(\tfrac{1}{2} + \nu - \mu, 1 + 2\nu, \xi\right), \tag{2.6}$$

where the Tricomi function $U(\alpha, \beta, \xi)$ is built from a linear combination of the usual confluent hypergeometric functions of the first kind:

$$\begin{aligned} U(\alpha,\beta,\xi) &= \frac{\Gamma(1-\beta)}{\Gamma(\alpha-\beta+1)} F(\alpha,\beta,\xi) \\ &+ \frac{\Gamma(\beta-1)}{\Gamma(\alpha)} \xi^{1-\beta} F(\alpha-\beta+1, 2-\beta, \xi), \end{aligned} \tag{2.7}$$

where $F(\alpha,\beta,\xi)$ is a hypergeometric series given by

$$F(\alpha,\beta,\xi) = 1 + \frac{\alpha}{\beta}\xi + \frac{\alpha(\alpha+1)}{\beta(\beta+1)}\frac{\xi^2}{2!} + ... \tag{2.8}$$

This construction ensures the desired decaying behavior at infinity: $U(\alpha,\beta,\xi) \to \xi^{-\alpha}$, $\alpha \in \mathbb{C}$.

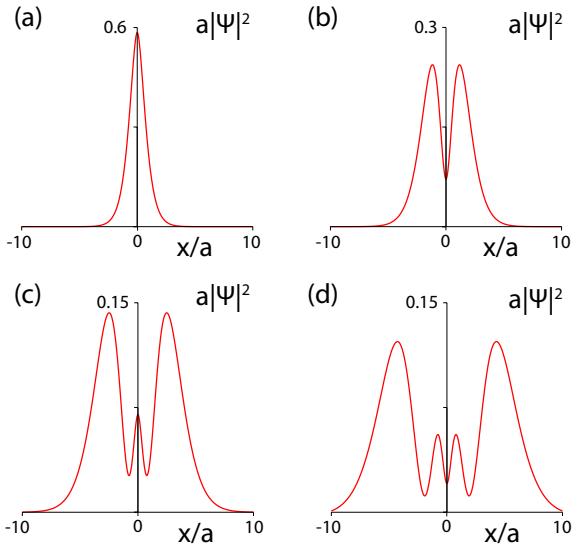

Figure 2.2: Probability density plots of the first four successive bound states with bandgap $\Delta a = 1$ and potential strength $U_0 = \frac{300}{137}$, where (a) $\varepsilon a = -0.248$, (b) $\varepsilon a = 0.350$, (c) $\varepsilon a = 0.570$ and (d) $\varepsilon a = 0.703$.

One can then proceed to find the full solution to the system of equations (2.2): in region II ($x > 0$) we obtain

$$\Psi_{II}(x) = \frac{c_{II}}{\sqrt{a}} \begin{pmatrix} W_{\mu,\nu}(\xi_{II}) \\ -\frac{\kappa+i\varepsilon}{\Delta} W_{\mu,\nu+1}(\xi_{II}) \end{pmatrix}, \tag{2.9}$$

similarly in region I ($x < 0$) it follows

$$\Psi_{I}(x) = \frac{c_{I}}{\sqrt{a}} \begin{pmatrix} \frac{\kappa+i\varepsilon}{\Delta} W_{\mu,\nu+1}(\xi_{I}) \\ W_{\mu,\nu}(\xi_{I}) \end{pmatrix}, \tag{2.10}$$

where now the variable $\xi_{I,II} = 2\kappa(a \mp x)$.

Using the continuity condition for both wavefunction components $\psi^{I}_{1,2}|_{x=0-} = \psi^{II}_{1,2}|_{x=0+}$ with Eq. (2.9) and Eq. (2.10), yields the ratio of constants $c_{II}/c_I = \pm i$, where c_I is found

via the normalization condition for a spinor wavefunction

$$\int_{-\infty}^{\infty} \left(|\psi_1|^2 + |\psi_2|^2\right) \mathrm{d}x = 1. \tag{2.11}$$

Bound state eigenvalues must be determined from the transcendental equation

$$\frac{\Delta}{\kappa + i\varepsilon} \frac{W_{\mu,\nu}(2\kappa a)}{W_{\mu,\nu+1}(2\kappa a)} = \pm i, \tag{2.12}$$

which can be solved graphically or via other standard root-finding methods. We show in Fig. 2.2 four illustrative electron density plots of the lowest bound states for $U_0 = \frac{300}{137}$, corresponding to a single charge Coulomb impurity on the axis of a single-walled carbon nanotube, and $\Delta a = 1$. Characteristically, the ground state density has a single peak, followed by two peaks for the first excited state, and so on. The value of the density at the origin alternates from being one of a local maxima to a local minima, but in a noticeable contrast to the non-relativistic case is never zero. This arises from the matrix nature of the Hamiltonian Eq. (2.1), which ensures both wavefunction components never vanish simultaneously. Higher energy bound states are more spread in space, with the highest peaks of probability density concentrated in the two outermost shoulders.

In the limit of $a \to 0$, a pure Coulomb potential is obtained. This limit leads to an unveiling of a signature of atomic collapse: at small a, the low energy eigenstates possess a higher than expected number of peaks, with the expected ground state (with single peak), first excited state (with double peak) and so on lost one after another from the bound state spectrum into the continuum as a further approaches zero.

2.1.3 The truncated Coulomb problem

We also consider the truncated 1D Coulomb potential, plotted in Fig. 2.3 and shaped by the piecewise function

$$V_t(x) = \begin{cases} -2U_0/d, & \text{if } |x| \le d/2 \\ -U_0/|x|, & \text{if } |x| > d/2 \end{cases} \tag{2.13}$$

where the Coulomb potential has been terminated at a radius $d/2$ to form a flat-bottom quantum well at small distances.

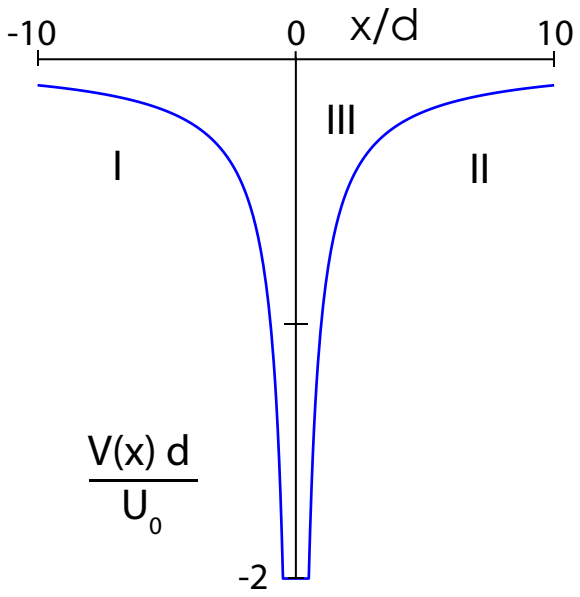

Figure 2.3: A plot of the truncated Coulomb potential, defined by Eq. (2.13).

In the exterior regions I and II, where $|x| > d/2$, the solutions follow from those of Sec. 2.1.2 upon setting $a = 0$. In the interior region III, where $|x| \leq d/2$, the solutions are simply

$$\Psi_{III}(x) = \frac{c_{III}}{\sqrt{a}} \begin{pmatrix} \sin(kx) \\ f_1(x) \end{pmatrix} + \frac{c_{IV}}{\sqrt{a}} \begin{pmatrix} \cos(kx) \\ f_2(x) \end{pmatrix}, \tag{2.14}$$

where we have introduced the auxiliary two-component function

$$\begin{pmatrix} f_1(x) \\ f_1(x) \end{pmatrix} = \frac{k}{\Delta} \begin{pmatrix} \cos(kx) \\ -\sin(kx) \end{pmatrix} + \frac{\varepsilon + 2U_0/d}{i\Delta} \begin{pmatrix} \sin(kx) \\ \cos(kx) \end{pmatrix}, \tag{2.15}$$

which necessitates the introduction of a new wavenumber $k = \sqrt{(\varepsilon + 2U_0/d)^2 - \Delta^2} > 0$, arising from the short-range behavior of the potential. The wavenumber defining the long-range decay of the wavefunction remains κ, introduced after Eq. (2.5). Together, requiring $k, \kappa > 0$, one finds a definite region in which confined states may form, restricted maximally by $|\varepsilon d| < \varepsilon_{max} d = \Delta d$ and minimally by $\varepsilon d > \varepsilon_{min} d = \Delta d - 2U_0$.

Imposing continuity on the wavefunction components at $x = \pm d/2$ leads to the following transcendental equation governing the energy quantization of bound states

$$1 - \lambda_+/\lambda_- = 0, \tag{2.16}$$

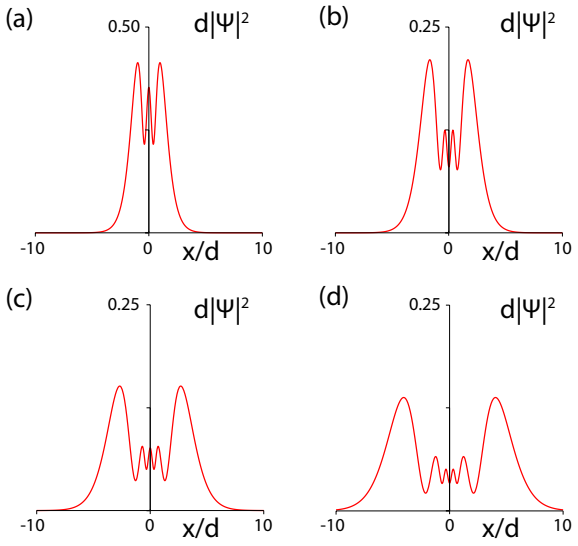

Figure 2.4: Probability density plots of the first four lowest bound states with bandgap $\Delta d = 1$ and potential strength $U_0 = \frac{300}{137}$, where (a) $\varepsilon d = -0.270$, (b) $\varepsilon d = 0.191$, (c) $\varepsilon d = 0.460$ and (d) $\varepsilon d = 0.623$.

where

$$\lambda_\pm = \frac{\frac{k}{\Delta\tau_\pm}\tan\left(\frac{kd}{2}\right) \pm \eta_\pm}{\eta_\pm \tan\left(\frac{kd}{2}\right) \mp \frac{k}{\Delta\tau_\pm}}, \tag{2.17}$$

$$\eta_\pm = i\left(\frac{\varepsilon + 2U_0/d}{\Delta\tau_\pm}\right) \mp 1, \tag{2.18}$$

$$\tau_\pm = \left(\frac{\kappa + i\varepsilon}{\Delta}\frac{W_{\mu,\nu+1}(\kappa d)}{W_{\mu,\nu}(\kappa d)}\right)^{\pm 1}, \tag{2.19}$$

which can be solved via the usual root-searching procedures. In Fig. 2.4 we plot electron densities for the four lowest bound states for $\Delta d = 1$ and $U_0 = \frac{300}{137}$. Most noticeable is the absence of the single-peaked and double-peaked electron densities (the naturally expected ground and first excited states). This is because for the chosen value of the bandgap there are no such solutions to Eq. (2.16) inside the allowed region of bound states, as represented graphically in Fig. 2.5 (where we show only the four lowest states for clarity). The critical bandgaps, below which the three lowest bound states are lost into the continuum, are $(\Delta d)_c = 1.86, 1.11, 0.57$. As one further decreases Δd successively higher bound states are lost one after another. The disappearance of low-lying states from the discrete spectrum is a generic feature of the Coulomb potential independent of its regularization at small distance: in the case of Sec. 2.1.2, one finds the lowest three states

merge with the continuum at $(\Delta a)_c = 0.56, 0.23, 0.10$.

Lower energy bound states diving into the continuum below the bandgap is a signature of the so-called atomic collapse [80, 81, 82]. Its appearance in 1D Dirac materials, with its dependence on critical bandgaps, opens a new avenue to explore such an exotic relativistic quantum mechanical phenomenon in a tabletop experiment. In fact, quasi-1D Dirac systems, like carbon nanotubes, are arguably more suitable for table-top experiments on atomic collapse than graphene. Unlike graphene with a 2D Coulomb potential, the system considered here contains a band gap, which can even be controlled by external electric [83, 84] or magnetic [85, 86, 87, 88] fields, and admits truly bound state solutions with square-integrable wavefunctions.

The results shown in Fig. 2.5 are somewhat similar to those found in graphene for bound states in a 1D square potential well extended infinitely in the y-direction, with the role of the bandgap being played by the transversal wavevector $\Delta \to k_y$ [89, 90]. The most important difference is that the Coulomb problem admits an infinitely large family of bound states for every nonzero size of the bandgap, albeit some shallower states may be missing for small bandgaps. In the square well, which is in fact of less practical relevance due to the difficulty in creating sharp potential barriers in realistic devices, as the bandgap gets smaller so does the finite number of bound states present beyond the continuum.

We should also mention the results presented here are qualitatively the same with changing U_0 (which could arise due to the dielectric environment or due to the renormalization of the Fermi velocity seen towards the Dirac point). The most prominent difference is the shape of the allowed region of confined states, due to the appearance of U_0 in the small-distance wavevector k.

2.1.4 Conclusion

We have presented the exact solutions to the quasi-relativistic shifted and truncated Coulomb problems for a quasi-relativistic 1D matrix Hamiltonian, which has a direct application to the growing research area of Dirac materials [6].

We have shown that manipulating the size of the bandgap allows one to exclude from the discrete spectrum certain low-lying quantum states, for example the ground state,

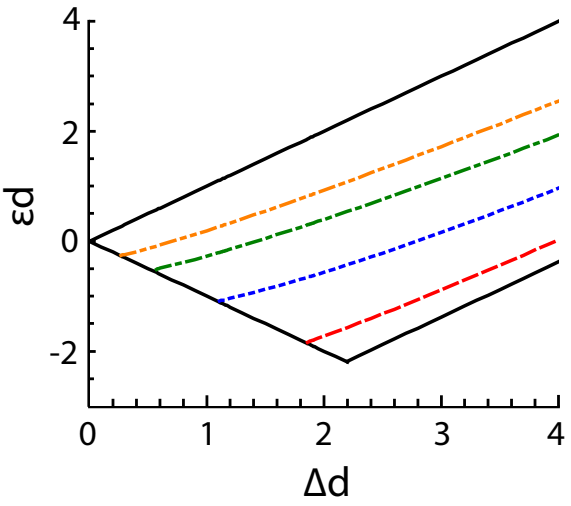

Figure 2.5: A plot of the dependence of the bound state energies on band gap for the lowest four states: the ground state (dashed red line), the first excited state (dotted blue line), the second state (dot-dashed green line) and the third state (dot-dot-dashed orange line) respectively, where $U_0 = \frac{300}{137}$. The solid black lines denote the region bound states must fall between.

in stark contrast to the non-relativistic case. The bandgap can be controlled, e.g. in the case of carbon nanotubes, by applying an external field [83, 84, 85, 86, 87, 88] or via strain [91]; or in graphene nanoribbons by choosing certain nanoribbons with a desirable geometry [92]. Alternatively, the strength of the interaction potential can be controlled by having multiple charged impurities [93] or changing the dielectric environment.

We hope some interesting features arising from Coulomb physics, such as atomic collapse effects, can soon be observed either in the currently known quasi-1D Dirac materials or in future crystals synthesized with the latest techniques [94].

2.2 Spatial modulations of the Fermi velocity

The particles found in Dirac materials are notorious for being difficult to manipulate due to the absence of backscattering. Here we investigate how spatial modulations of the Fermi velocity of Dirac particles can give rise to localization effects in one dimensions, and a generalization to two dimensions is also possible. We present several exactly solvable models illustrating the nature of the bound states which arise.

2.2.1 Introduction

There is a considerable resurgence in the importance of the Dirac equation in condensed matter physics due to the rise of so-called Dirac materials, whose charge carriers behave according to quasi-relativistic wave equations [6]. Celebrated examples include the surface states of topological insulators or graphene. One important property that directly follows is the absence of backscattering [9], which whilst leading to large electron mobilities, provides a difficulty in localizing Dirac electron and so building a practical, digital devices [68].

One interesting method proposed to manipulate the somewhat elusive quasi-relativistic charge carriers is to consider systems with a spatially varying Fermi velocity [95, 96]. The resulting ballistic electron transport has already been extensively studied [97, 98, 99, 100], as has the effects of applying external electric [101] and magnetic fields [102] and a superlattice [103]. There are immediately apparent strong analogies in both acoustics and especially optics, where phenomena such as supercollimation can be envisaged [104, 105]. We should also mention velocity engineering of bilayer graphene has been investigated [106].

Energy varying Fermi velocity renormalization has already been seen in experiments at energies close to the Dirac point [107, 108]. Here we consider the problem of Dirac particles that can be described with a spatially modulated Fermi velocity $v_F = v_F(\mathbf{r})$, which arises theoretically from both elasticity theory with tight-binding as well as quantum field theory in curved space [109]. Experimentally, a spatially dependent velocity may occur due to ripples in the material [110], the use of an SiO_2 substrate[111], superlattices [29, 112, 113], atomic scale defects induced by ion irradiation [114], straining

the material directly grown on a a substrate such as h-BN [115], or by placing a grounded plane of metal nearby [98]. Indeed, a spatial dependence of the Fermi velocity has already been noticed [113].

Previously, most of the attention has been focused on the scattering of massless Dirac fermions on square velocity barriers, either single [102] or double [116], however here we address the bound state problem on non-square velocity distributions.

It has been shown by Peres [96] that in order to maintain Hermitian operators, the relevant (and Sturm-Liouville) Dirac Hamiltonian is

$$\hat{H} = \sqrt{v_F(\mathbf{r})}\boldsymbol{\sigma}\cdot\hat{\mathbf{p}}\sqrt{v_F(\mathbf{r})}, \tag{2.20}$$

where $\boldsymbol{\sigma} = (\sigma_x, \sigma_y)$ are the (pseudo)spin matrices of Pauli. Eq. (2.20) is acted upon by a two-component spinor wavefunction, $\Phi(\mathbf{r})$. Continuity of the probability current leads to the boundary condition at an interface $\mathbf{r} = \mathbf{R}$

$$\sqrt{v_F(\mathbf{r})}\Phi(\mathbf{r})\Big|_{\mathbf{r}=\mathbf{R}+\boldsymbol{\delta}} = \sqrt{v_F(\mathbf{r})}\Phi(\mathbf{r})\Big|_{\mathbf{r}=\mathbf{R}-\boldsymbol{\delta}}, \tag{2.21}$$

which is analogous to what occurs in heterostructures defined by a position dependent mass. In what follows, we make the following assignment of the auxiliary spinor for convenience $\Psi(\mathbf{r}) = \sqrt{v_F(\mathbf{r})}\Phi(\mathbf{r})$. Let us make the ansatz $\Psi(x,y) = (L_y)^{-1/2}e^{iq_y y}\left(\begin{smallmatrix}1 & 0\\ 0 & i\end{smallmatrix}\right)\psi(x)$, where the spinor $\psi(x) = [\psi_1(x), \psi_2(x)]^T$, due to translational invariance in the y direction. We shall consider several toy models of 1-D velocity barriers in what follows, with drastically different spatial profiles, as shown in Fig. 2.6.

2.2.2 The square velocity barrier

Firstly, we revisit the square model [96, 97, 98, 99] velocity barrier of width d

$$v(x) = \begin{cases} v_0, & -\frac{d}{2} \le x \le \frac{d}{2} \\ v_1, & x > \frac{d}{2}, \quad x < -\frac{d}{2} \end{cases} \tag{2.22}$$

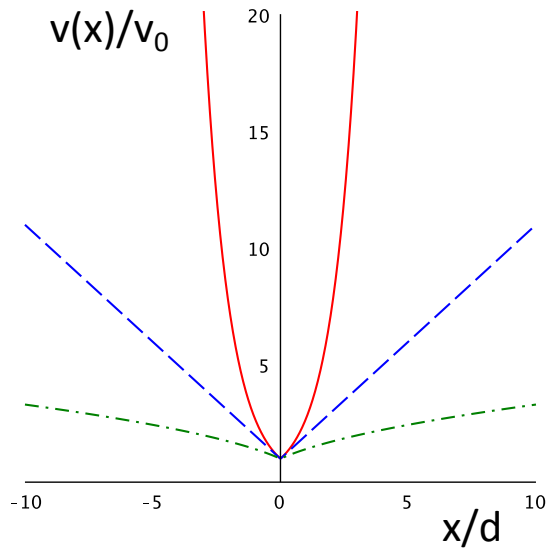

Figure 2.6: Profiles of the velocity barriers considered, namely the exponential barrier (solid red line), linear barrier (dashed blue line) and square root barrier (dotted green line).

where $v_1 > v_0$. There has been much focus on scattering on such a barrier, instead we shall investigate the associated bound states. Naturally appearing in this problem are the wavevectors

$$\kappa = \left(q_y^2 - \left(\tfrac{E}{\hbar v_1}\right)^2\right)^{1/2}, \quad k = \left(\left(\tfrac{E}{\hbar v_0}\right)^2 - q_y^2\right)^{1/2} \tag{2.23}$$

which arise when describing the wavefunction in its evanescent and propagating stages respectively. These wavevectors automatically restrict the region of bound states to the fan $\hbar v_0|q_y| < |E| < \hbar v_1|q_y|$. The energies of the bound states are determined by

$$\tan(kd) = \frac{2\frac{v_1}{v_0}\frac{\kappa}{k}}{1 + \left(1 - \frac{v_1}{v_0}\right)^2\left(\frac{q_y}{k}\right)^2 - \left(\frac{v_1}{v_0}\frac{\kappa}{k}\right)^2}. \tag{2.24}$$

As is common in one-dimensional barrier problems, there is always at least one bound state, even for arbitrarily weak barriers as $v_0/v_1 \to 1$. Upon taking this limit, one can see from Eq. (2.24) that the left hand side of the equation will grow monotonically between $0 \leq \tan(kd) \leq \left(v_1^2/v_0^2 - 1\right)^{1/2} q_y d$, which will always be intercepted as the right hand side tends to zero as $|E| \to \hbar v_1|q_y|$.

In the opposite limit $v_0/v_1 \to 0$, Eq. (2.24) reduces to $\tan(kd) + k/q_y = 0$. Now

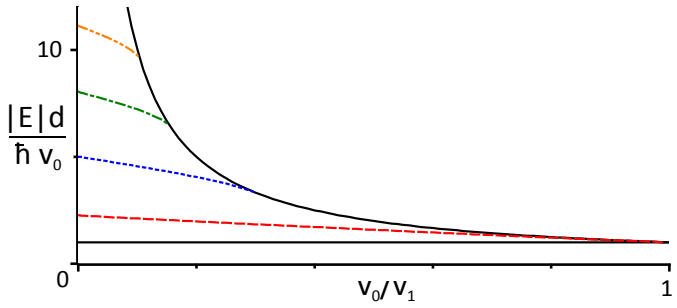

Figure 2.7: Eigenvalue spectrum of Dirac fermions in a square velocity barrier. The lowest four states are shown, from the ground state (dashed red line), to higher states (dotted blue line, dash-dot green line, dash dot-dot orange line). The region of allowed bound states is denoted by a solid black line. Here we take $q_y d = 1$.

there are an increasing number N of bound states, which can be estimated from

$$N = \left\lfloor \Upsilon \frac{q_y d}{\pi} \right\rfloor, \quad \Upsilon = \left(v_1^2 / v_0^2 - 1 \right)^{1/2} \tag{2.25}$$

where $\lfloor ... \rfloor$ is the floor function. Inverting Eq. (2.25) tells us the threshold velocity barrier strengths above which new bound states appear, via the approximate relation $v_0/v_1 = \left(1 + \left(N q_y d/\pi\right)^2\right)^{-1/2}$. These features can been seen from the numerical solutions to Eq. (2.24), which we plot in Fig. 2.7.

2.2.3 The exponential velocity barrier

Let us study the exponential velocity barrier, plotted in Fig. 2.6 and defined by

$$v(x) = v_0 e^{|x|/d}, \tag{2.26}$$

where v_0 is the minimal Fermi velocity, found at the center of the barrier, and d is the length scale of the problem, from which arises the key dimensionless parameter

$$\lambda = \frac{|E|d}{\hbar v_0}. \tag{2.27}$$

Upon solving the coupled Eqs. (2.20) one finds the following wavefunction in region I ($x > 0$)

$$\psi^I(x) = \frac{c_I}{\sqrt{d}} e^{-x/2d} \begin{pmatrix} J_{qd+1/2}\left(\lambda e^{-x/d}\right) \\ \mathrm{sgn}(E) J_{qd-1/2}\left(\lambda e^{-x/d}\right) \end{pmatrix}, \tag{2.28}$$

in terms of the Bessel function of the first kind $J_\alpha(\xi)$. The solution in region II ($x < 0$) is found by interchanging the top and bottom wavefunction components, and making the replacements $x \to -x$ and $c_I \to c_{II} = \pm \mathrm{sgn}(E) c_I$. Applying the boundary condition Eqs. (2.21), one finds the spectrum of bound states is determined via the transcendental equation

$$J_{qd-1/2}(\lambda) = \pm J_{qd+1/2}(\lambda), \tag{2.29}$$

which can be solved with standard root-finding methods or indeed graphically. However, upon taking the limit $q \to 0$ one arrives at the analytic expression,

$$E_n = \pm\pi\left(n + \tfrac{1}{4}\right)\frac{\hbar v_0}{d}, \quad n = 0, \pm 1, \pm 2, \ldots \tag{2.30}$$

from which one notices there is a threshold energy of $\lambda = \pi/4$ before one can reach the first bound state.

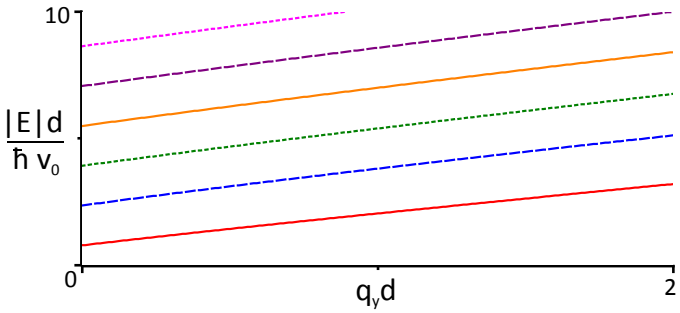

Figure 2.8: Progression of the six lowest bound states energies with traversal momentum for Dirac particles in an exponential velocity barrier.

The solutions to Eq. (2.29) are presented in Fig. 2.8: in the regime shown the energy bands can be approximated as linearly growing with wavevector, explicitly

$$\frac{|E_N|d}{\hbar v_0} = \frac{\pi}{4}(2N-1) + \left(\frac{N/5+5}{4}\right) q_y d, \quad N = 1, 2, \ldots \tag{2.31}$$

which is especially reasonable for $N > 1$.

2.2.4 The linear velocity barrier

Now we will look at the linear velocity barrier, sketched in Fig. 2.6 and shaped by

$$v(x) = v_0(1 + |x|/d), \tag{2.32}$$

and we define the useful dimensionless quantity

$$\gamma = \frac{Ed}{\hbar v_0}. \tag{2.33}$$

Proceeding in a similar manner to Sec. 2.2.3, one finds the wavefunction in region I ($x > 0$) is

$$\psi^I(x) = \frac{c_I}{\sqrt{d}}\left(1 + \frac{x}{d}\right)^{i\gamma} e^{-qx} \times \begin{pmatrix} U\left(1 + i\gamma, 1 + 2i\gamma, 2qd(1 + \frac{x}{d})\right) \\ \gamma^{-1}U\left(i\gamma, 1 + 2i\gamma, 2qd(1 + \frac{x}{d})\right) \end{pmatrix}, \tag{2.34}$$

where $U(\alpha, \beta, \xi)$ is the Tricomi function or confluent hypergeometric equation of the second kind [79]. The solution in region II ($x < 0$) is found by interchanging the top and bottom wavefunction components, and making the replacements $x \to -x$ and $c_I \to c_{II} = \pm c_I$. Ensuring a conserved probability current yields the eigenvalues equation

$$U\left(i\gamma, 1 + 2i\gamma, 2qd\right) = \pm\gamma U\left(1 + i\gamma, 1 + 2i\gamma, 2qd\right), \tag{2.35}$$

which, although it must be solved numerically, can be solved with any desired accuracy, as shown in Fig. 2.9. Most noticeable is the absence of threshold bound state energies as $q_y d \to 0$, markedly different from the sharper cusp profile of Sec. 2.1.2.

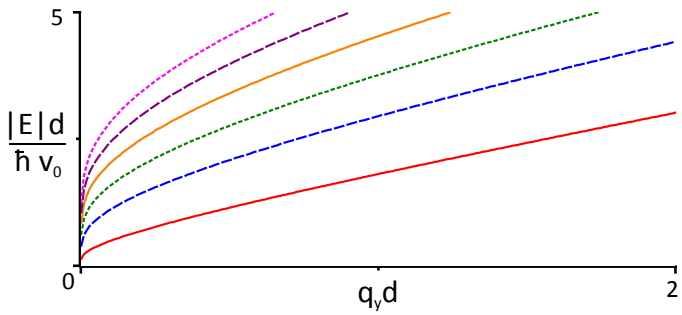

Figure 2.9: Progression of the six lowest bound states energies with traversal momentum for Dirac particles in a linear velocity barrier.

2.2.5 The square root velocity barrier

Finally, we consider a weakly growing square root velocity barrier, graphed in Fig. 2.6 and with the functional form

$$v(x) = v_0 \sqrt{1 + |x|/d}. \tag{2.36}$$

One may obtain the wavefunction in region I ($x > 0$) as

$$\psi^I(x) = \frac{c_I}{\sqrt{d}} \left(1 + \tfrac{x}{d}\right)^{1/2} e^{-qx} \times \begin{pmatrix} U\left(1 - \frac{\gamma^2}{2qd}, \frac{3}{2}, 2qd(1 + \frac{x}{d})\right) \\ \gamma^{-1} (2qd)^{1/2} U\left(\frac{1}{2} - \frac{\gamma^2}{2qd}, \frac{3}{2}, 2qd(1 + \frac{x}{d})\right), \end{pmatrix} \tag{2.37}$$

whilst the solution in region II ($x < 0$) is found by interchanging the top and bottom wavefunction components, and making the replacements $x \to -x$ and $c_I \to c_{II} = \pm c_I$. The eigenvalues are governed by

$$\gamma^{-1} (2qd)^{1/2} U\left(\tfrac{1}{2} - \tfrac{\gamma^2}{2qd}, \tfrac{3}{2}, 2qd\right) = \pm U\left(1 - \tfrac{\gamma^2}{2qd}, \tfrac{3}{2}, 2qd\right), \tag{2.38}$$

which is tractable with standard root-searching procedures, the result of which is shown in Fig. 2.10.

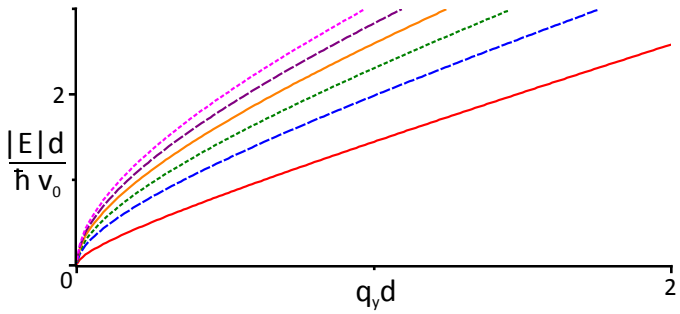

Figure 2.10: Progression of the six lowest bound states energies with traversal momentum for Dirac particles in a square root velocity barrier.

Upon comparing Fig. 2.8, Fig. 2.9 and Fig. 2.10 one notices as the velocity barrier becomes shallower the bound state energies lower and the inter-energy spacing reduces, whilst as soon as the velocity barrier is not growing fast (exponentially) there is no threshold as $q_y d \to 0$.

2.2.6 Conclusion

We have calculated the nature of the bound states that arise in several different velocity barrier configurations in 1-D geometries. We have shown how velocity barriers (growing slower than exponential) support bound modes for arbitrarily small transversal wavevectors. These results open up an avenue to explore in the quest to acheive digital switching behavior with Dirac particles.

Chapter 3

Two dimensional problems

I call our world Flatland, not because we call it so, but to make its nature clearer to you, my happy readers, who are privileged to live in Space.

- *Edwin A. Abbott*

3.1 Magnetic quantum dots and rings

We show how it is indeed possible to trap two-dimensional massless Dirac fermions in both magnetic quantum dots and rings. Crucially, the spatial decay at infinity of the magnetic field must be slower than the inverse square of the radial distance. It is also found one sign of the electron angular momentum is excluded depending on the sign of the field. We illustrate these characteristics with both exact solutions and a hitherto unknown quasi-exactly solvable model based on confluent Heun functions.

3.1.1 Introduction

Inhomogeneous magnetic fields continue to play an important role in modern physics, from the classic Stern-Gerlach experiment [117] of 1922 to the post-World War II achievements in magnetic confinement of plasmas in tokamaks [118] and the more recent magnetic levitation of macroscopic objects [119].

With the rise of the two-dimensional Dirac material graphene, whose electrons behave like massless Dirac fermions, the influence of magnetic fields has been pivotal to research into fundamental physics, including relativistic Landau levels [120, 121, 122], Fock-Darwin states [123], integer [124] and fractional [125] quantum Hall effects and quantum spin Hall states [126].

An important feature of Dirac fermions is the complete absence of backscattering [9], leading to a great difficulty in confining electrons electrostatically [127]. Therefore, much effort has been expounded on considerations of magnetic traps [128, 129]. One-dimensional magnetic confinement has been shown to be key for snake states [130, 131] and many inhomogeneous field profiles have been treated [132, 133, 134, 135, 136, 137]. Zero-dimensional confinement in perpendicular magnetic fields has also been treated extensively [138], with magnetic antidots [139] and antirings [140, 141] (where the magnetic field is zero inside the dot and ring) being shown to confine electrons but magnetic dots [142] (where the magnetic field is nonzero inside the dot) has been shown to not support bound states. In fact, as long as the magnetic trap decays at infinity slower than $1/r^2$, bound states are indeed possible in both magnetic dots and rings as an asymptotic reduction of the wavefunction to non-square-integrable Bessel functions is avoided. Am-

biguities found in the case of a pure scalar potential decaying as $1/r^2$ are avoided because of the structure of the quasi-relativistic equations in two-dimensions [143, 144].

Here we discuss several examples of magnetic profiles which show confinement in magnetic quantum dots and rings. Notably, we study more realistic magnetic fields than the well-known square-well model [139], which are both inhomogeneous and regular at the origin. In doing so, we make use of both exact solutions and quasi-exactly solvable (QES) models [65], which most clearly display the underlying physics.

Experimentally, nonuniform magnetic fields can be created by either deposition of ferromagnetic microstructures [145] or superconducting stripes on top of the two-dimensional electron gas [146], or by curving the membrane [147].

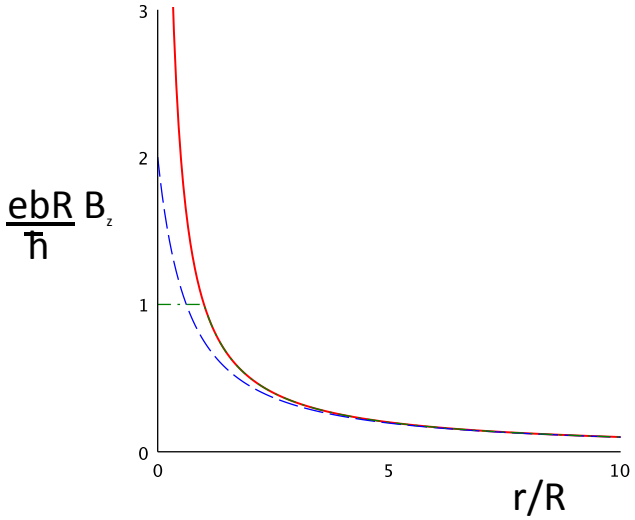

Figure 3.1: A plot of the non-uniform magnetic field profiles considered, comprised of a singular profile (solid red line), a regularized profile (green dash-dot line) and a smooth profile (blue dotted line).

The single particle Hamiltonian describing the two-dimensional excitations in graphene and other such Dirac materials in a magnetic field can be written

$$\hat{H} = v_{\mathrm{F}}\boldsymbol{\sigma}\cdot(\hat{\boldsymbol{p}} + e\boldsymbol{A})\,, \tag{3.1}$$

where v_F is the Fermi velocity, $\boldsymbol{\sigma}$ are Pauli's spin matrices and $\boldsymbol{A}$ is a magnetic vector

potential. Acting on this Hamiltonian with a wavefunction of the form

$$\Psi(r,\theta) = \frac{e^{im\theta}}{\sqrt{2\pi}} \begin{pmatrix} \chi_A(r) \\ ie^{i\theta}\chi_B(r) \end{pmatrix}, \quad m = 0, \pm 1, \pm 2, ... \tag{3.2}$$

leads to the following coupled equations

$$\left(\partial_r + \tfrac{m+1}{r} + \tfrac{e}{\hbar}A_\theta\right)\chi_B = \varepsilon\chi_A, \tag{3.3a}$$

$$\left(-\partial_r + \tfrac{m}{r} + \tfrac{e}{\hbar}A_\theta\right)\chi_A = \varepsilon\chi_B, \tag{3.3b}$$

where the eigenvalue $E = \hbar v_F \varepsilon$ and the magnetic field $B_z = r^{-1}\partial_r(rA_\theta(r))$ enters via the vector potential. We start by noting the problem of a Dirac fermion in a singular magnetic field [148], with the spatial inhomogeneity

$$B_z(r) = \frac{\hbar}{e}\frac{1}{br}, \tag{3.4}$$

where b is a length which effectively describes the magnitude of the field, can be solved exactly. Upon reducing the system of equations Eqs. (3.3) to a single Schrödinger equation for wavefunction component χ_B only, one finds a formal identification with the two-dimensional hydrogen atom [42], such that one can write down the eigenenergy spectrum

$$\varepsilon_{n,m} b = \pm\left\{1 - \left(\frac{1+2m}{1+2n+2|m+1|}\right)^2\right\}^{1/2}, \tag{3.5}$$

$$m \leq -1, \quad n = 0, 1, 2...$$

It is interesting how one may exclude one sign of angular momenta, and the dependence on both quantum numbers n and m. However, this singular field model is somewhat unphysical. Therefore, we study a smooth, regular profile in Sec. 3.1.2, and consider toy models of a magnetic quantum dot and ring in Sec. 3.1.3 and Sec. 3.1.4 respectively. Finally, we draw some conclusions in Sec. 3.1.5.

3.1.2 A quasi-exactly solvable model

Remarkably, a further counterexample of unexpected beauty can be found in the following QES, please consider

$$B_z(r) = \frac{\hbar}{e}\frac{1}{bR}\frac{2 + r/R}{(1 + r/R)^2}. \tag{3.6}$$

We seek the lower wavefunction component in the form

$$\chi_B = \tfrac{c}{R} \times \xi^{|m+1+R/b|} e^{-\kappa\xi} w(\xi), \tag{3.7}$$

with c a normalization constant and we use the notation

$$\xi = r/b, \quad \kappa = (1 - \varepsilon^2 b^2)^{1/2}. \tag{3.8}$$

This is reasonable, since we know the behavior of the function as $\xi \to 0$ should be $\chi_B \sim \xi^{|m+1+R/b|}$, and the exponential decrease ($e^{-\kappa\xi}$) as $\xi \to \infty$. Substitution of Eq. (3.7) into Eq. (3.3) and elimination of χ_A yields the equation

$$\begin{aligned} &w''(\xi) + 2|m + 1 + t^{-1}|\xi^{-1} w'(\xi) \\ &\qquad - \Big(\frac{\kappa(1 + 2|m + 1 + t^{-1}|) + 1 + 2m}{z} \\ &- \frac{t^2 + 2t(m + 1)}{z^2} + \frac{2(tz)^{-1}}{1 + 2t} - \frac{z^{-1}}{(1 + tz)^2} + \frac{2t^{-1}(1 + m)z^{-2}}{1 + tz} + \frac{(tz)^{-2}}{(1 + tz)^2}\Big) w(\xi) = 0, \quad t = b/R, \end{aligned} \tag{3.9}$$

where the prime denotes differentiation with respect to ξ. We introduce a new independent variable $\zeta = -\frac{b}{R}\xi$ and take the ansatz

$$w(\zeta) = (1 - \zeta)^{R/b} g(\zeta), \tag{3.10}$$

to obtain a form of the confluent Heun equation [149]

$$g''(\zeta) + \left(\alpha + \tfrac{\beta+1}{\zeta} + \frac{\gamma + 1}{\zeta - 1}\right) g'(\zeta) + \left(\tfrac{\mu}{\zeta} + \tfrac{\nu}{\zeta-1}\right) g(\zeta) = 0, \tag{3.11}$$

$$\mu = \tfrac{1}{2}(\alpha - \beta - \gamma + \alpha\beta - \beta\gamma) - \eta, \nu = \tfrac{1}{2}(\alpha + \beta + \gamma + \alpha\gamma + \beta\gamma) + \delta + \eta, \tag{3.12}$$

with parameters

$$\alpha = 2\tfrac{R}{b}\kappa, \quad \beta = 2|m+1+\tfrac{R}{b}|, \gamma = 2\tfrac{R}{b} - 1, \quad \delta = \tfrac{R}{b}(1+2m), \quad \eta = \tfrac{1}{2}. \tag{3.13}$$

The Frobenius solution to Eq. (3.11) is computed as a power series expansion around the origin $\zeta = 0$, a regular singular point, with a radius of convergence $|\zeta| < 1$

$$g(\zeta) = \sum_{n=0}^{\infty} v_n(\alpha,\beta,\gamma,\delta,\eta,\zeta)\zeta^n = H_c(\alpha,\beta,\gamma,\delta,\eta,\zeta), \tag{3.14}$$

where the coefficients v_n satisfy a three term recurrence relation. This confluent Heun function $H_c(\zeta)$ must reduce to a polynomial, since otherwise it would increase exponentially as $\xi \to \infty$. The function $H_c(\zeta)$ reduces to a polynomial if two conditions are met [66]. Firstly, $\frac{\delta}{\alpha} + \frac{1}{2}(\beta+\gamma) + N + 1 = 0$, or equivalently

$$\varepsilon^{QES}_{N,m} b = \pm\left\{1 - \left(\frac{m+\frac{1}{2}}{N+\frac{1}{2}+\frac{R}{b}+|m+1+\frac{R}{b}|}\right)^2\right\}^{1/2}, m \leq -1, \quad N = 1, 2... \tag{3.15}$$

which ensures the $(N+1)$th coefficient in the series expansion is a polynomial in η of order $N+1$. Then the second necessary condition is to find some value of δ that is a root of that polynomial, such that the coefficient v_{N+1} is zero and hence (due to the recurrence relationships) all successive coefficients are also zero. Then the series has been truncated and $H_c(\zeta)$ is simply a confluent Heun polynomial.

As an example, consider the $m = -2$ state and set $R/b = 1$. Then one finds from Eq. (3.15), the energy levels of the first few QES modes $\varepsilon_{1,-2}b = \pm 0.824$, $\varepsilon_{2,-2}b = \pm 0.913$ and $\varepsilon_{3,-2}b = \pm 0.948$. Upon solving for the roots of the resultant quadratic, cubic and quartic equations respectively in δ, one finds $b = 0.931, 0.915, 0.948$ respectively. We plot in Fig. 3.2 these example probability densities. Thus we have found in a realistic, regularized model truly bound modes of Dirac-Weyl excitations can exist.

It is not surprising, yet still rather beautiful, that the QES system presented here has a directly analogous QES model in the framework of the 2D Schrödinger equation. In the

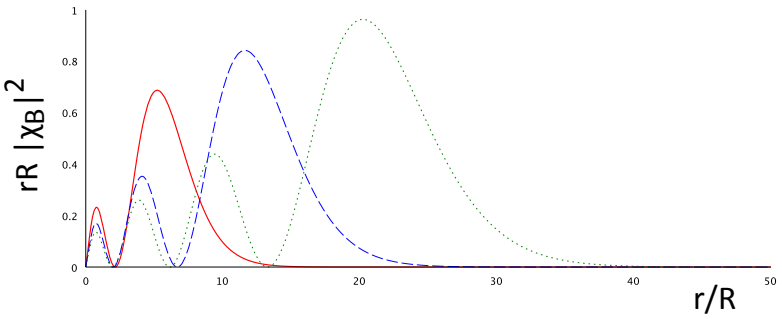

Figure 3.2: Probability density plots of the lower wavefunction component in the QES model considered, with state $m = -2$ and parameter $R/b = 1$. We display a first excited state $N = 1$ (solid red line), second excited state $N = 2$ (dashed blue line) and third excited state $N = 3$ (dotted green line).

non-relativistic case, the wavefunction and QES energy levels are instead given by

$$\Psi(r,\theta) = e^{im\theta} r^{|m+\frac{R}{b}|}(1 + r/R)^{1/2-\lambda} e^{-\frac{\kappa r}{b}} \times$$
$$H_c\left(2\kappa\tfrac{R}{b}, 2|m + \tfrac{R}{b}|, -2\lambda, 2m\tfrac{R}{b}, \tfrac{1}{2}, -\tfrac{r}{R}\right),\ \lambda = \left(\tfrac{R^2}{b^2} + \tfrac{1}{4}\right)^{\frac{1}{2}}, \quad (3.16)$$

where we have redefined $\kappa = (1 - \varepsilon b^2)$ and now our particle of mass M has an effective eigenvalue $\varepsilon = 2ME/\hbar^2$, explicitly

$$\varepsilon^{QES}_{N,m} b^2 = \left\{1 - \left(\frac{m}{1 + N + |m + \frac{R}{b}| - \lambda}\right)^2\right\}^{1/2}. \quad (3.17)$$

Further, rather intriguing results in the non-relativistic regime are the subject of future study.

3.1.3 A magnetic quantum dot

Let us consider a magnetic quantum dot, defined by

$$B_z(r) = \frac{\hbar}{e}\frac{1}{b}\begin{cases} R^{-1}, & r \le R, \quad \text{(region I)} \\ r^{-1}, & r > R. \quad \text{(region II)} \end{cases} \quad (3.18)$$

where we have introduced the second length scale R, which is in immediate competition with b. The solutions in region I are the well known relativistic level Landau wavefunc-

tions [122], which can be given in terms of Kummer's function $F(a,b,z)$ as

$$\chi_B^I = \tfrac{c_I}{b} \times r^{|m+1|} e^{-\frac{r^2}{4bR}} F(a_I, b_I, \tfrac{r^2}{2bR}), \tag{3.19}$$

$$a_I = \tfrac{1}{2}\left(1 + m + |1+m| - \varepsilon^2 bR\right), \quad b_I = 1 + |1+m|,$$

and the upper wavefunction component χ_A can be easily found from Eq. (3.3a). The wavefunctions in region II are similar to those of the problem in Sec. 3.1.2, explicitly

$$\chi_B^{II} = \tfrac{c_{II}}{b} \times (r/b)^{|m+1|} e^{-\frac{\kappa r}{b}} U(a_{II}, b_{II}, \tfrac{2\kappa r}{b}), \tag{3.20}$$

$$a_{II} = \tfrac{1}{2} + |1+m| + \tfrac{2m+1}{2\kappa}, \quad b_{II} = 1 + 2|1+m|,$$

except here we choose instead the second linearly independent solution to Kummer's equation $U(a,b,z)$ [79], in order to have a square-integrable wavefunction at infinity. Enforcing both wavefunction components to be continuous across the interface at $r = R$, one obtains the matching constant

$$\frac{c_{II}}{c_I} = e^{\frac{R}{b}\left(\kappa - \frac{1}{4}\right)} \frac{F(a_I, b_I, \frac{R}{2b})}{U(a_{II}, b_{II}, \frac{2\kappa R}{b})}, \tag{3.21}$$

and the following transcendental equation for energy quantization to be solved by root-finding methods

$$\frac{a_I}{b_I} \frac{F(a_I+1, b_I+1, \frac{R}{2b})}{F(a_I, b_I, \frac{R}{2b})} + 2\kappa a_{II} \frac{U(a_{II}+1, b_{II}+1, \frac{2\kappa R}{b})}{U(a_{II}, b_{II}, \frac{2\kappa R}{b})} + \kappa - 1 = 0, \tag{3.22}$$

which interpolates between two analytic functions in the limiting cases of (i) a singular field, governed by Eq. (3.5) in the regime $R/b << 1$; and (ii) a constant field, with relativistic Landau levels

$$\varepsilon_{n,m} (bR)^{1/2} = \pm \left(1 + m + |1+m| + 2n\right)^{1/2}, \quad R/b >> 1. \tag{3.23}$$

such that there is a transition depending on R/b at which one sign of angular momentum is excluded. Eq. (3.23) fully describes how the energy levels can be tuned at will depending

on the parameters of the magnetic quantum dot.

3.1.4 A magnetic quantum ring

It is straightforward to adapt the problem magnetic dot problem of Sec. 3.1.3 to describe a toy model of a magnetic quantum ring, defined by

$$B_z(r) = \frac{\hbar}{e}\frac{1}{br}\Theta(r-R), \tag{3.24}$$

where $\Theta(z)$ is Heaviside's step function. Now, inside the ring $r \leq R$ we have the usual free particle solution in terms of a Bessel function of the first kind $\chi_B^I = \frac{c_I}{b} J_{|m+1|}(\varepsilon r)$, and outside the ring $r > R$ we again have a wavefunction component like Eq. (3.20). Matching both wavefunction components at the ring boundary $r = R$ yields the following transcendental equation for the allowed eigenvalues

$$2\kappa a_{II}\frac{U(a_{II}+1, b_{II}+1, \frac{2\kappa R}{b})}{U(a_{II}, b_{II}, \frac{2\kappa R}{b})} - \varepsilon b\frac{J_{|m+1|+1}(\varepsilon R)}{J_{|m+1|}(\varepsilon R)} + \kappa - 1 = 0. \tag{3.25}$$

Solutions of Eq. (3.25) show how, even in a true ring with decaying field asymptotically, bound states exist and their dependence on the parameters of the system.

3.1.5 Conclusion

The problem of confinement of Dirac-Weyl particles in nonuniform magnetic fields has been considered. We have shown, with magnetic field profiles including examples of magnetic quantum dots and rings, how such traps should be of a short-range nature and how one sign of angular momentum is removed. We hope experimental realization of such magnetic confinement can be realized in the near future.

Furthermore, in graphene certain configurations of strain can lead to pseudomagnetic fields, which conserve time-reversal symmetry across the two valleys K and K'. Thus our results suggest to achieve bound states mechanically one needs to create very delicate strain configurations, not giving rise to short-range magnetic fields decaying at or faster than $1/r^2$. Also, the sign of the effective magnetic field will be opposite in the two valleys, giving rise to states rotating only with positive angular momentum in one valley

and only negative angular momentum in the other valley. This could be utilized in future mesoscopic devices.

3.2 Zero-energy states with and without a magnetic flux

The formation of bound states in Dirac materials is a highly nontrivial task due to the suppression of backscattering for chiral electrons with a Berry phase of π. Indeed, it is widely claimed confinement via purely electrostatic means is impossible. Here we provide a caveat to this belief by demonstrating theoretically bound states can arise at the Dirac point with only a scalar potential. We also propose to add a magnetic flux tube to the system, the modulation of which can be used as a tool to bring about confinement or deconfinement as required.

3.2.1 Introduction

Since the early days of graphene physics the phenomena of Klein tunneling [31, 150, 151] has led to the belief that no electric field can trap a bound state in graphene. Instead, proposals for magnetic confinement were put forward [123, 127, 139, 152, 153] and much work was carried out on the Aharonov-Bohm effect and graphene rings theoretically [154, 155, 155, 156] and later experimentally [158, 159].

However at the Dirac point, so-called zero-energy bound states may form at the apex of the Dirac cone. Mathematically, this is because at finite energy the effective Schrödinger equation at long range maps on to the problem of scattering states in a non-relativistic system (with solutions decaying like the square root of distance); whereas at zero energy solutions exist which decay algebraically (depending on the angular momentum quantum number m). When m is nonzero the solutions are fully square-integrable, such that they are rotating ring-like states, which always avoid the Klein tunnelling due to their vorticity resulting in a nonzero momentum component along the potential barrier.

Here, we show how to confine zero-energy states electrostatically and suggest magnetic flux as a way to deconfine electrons trapped in the purely electrostatic quantum dot or ring. Truly bound zero-energy states in graphene [160] are of great importance in transport phenomena [68, 161], and in so-called optimal traps, where the strength of the confining potential needs to be finely tuned. More abstractly, zero-modes of the Dirac equation are of enormous interest due to peculiar phenomena that have been associated with them, such as fractional charge [162] or Majorana excitations [163]. Here our model

potential holding zero-energy states is short-range, in stark contrast to the Coulomb potential [55, 164, 165, 166, 167], due to the requirement of a gate in all experiments.

To deconfine these bound modes, we propose to utilize magnetic flux tubes [168, 169]. Magnetic flux tubes have led to some interesting results in some exotic areas of physics, including superstring theory [170] and black hole pair production [171], as well as in condensed matter physics, for example in weak localization measurements [172].

3.2.2 Applying a magnetic flux tube

The single particle Hamiltonian describing electrons in graphene is of a Dirac-Weyl type

$$\hat{H} = v_{\mathrm{F}}\boldsymbol{\sigma}\cdot\hat{\boldsymbol{p}} + V(r), \tag{3.26}$$

where v_F is the graphene Fermi velocity and $\boldsymbol{\sigma}$ are Pauli's spin matrices. Acting with this Hamiltonian on a wavefunction of the form

$$\Psi(r,\theta) = \frac{Ce^{im\theta}}{\sqrt{2\pi}}\begin{pmatrix} \chi_A(r) \\ ie^{i\theta}\chi_B(r) \end{pmatrix}, \tag{3.27}$$

where $m = 0, \pm1, \pm2, ...$ and C is a normalization constant, separates the variables. A flux tube can be defined by the vector potential $\boldsymbol{A} = (0, A_\theta, 0)$, where

$$A_\theta(r) = \frac{\hbar}{e}\frac{f}{r}, \tag{3.28}$$

and $f = \Phi/\Phi_0$ is the number of flux quanta ($\Phi_0 = h/e$). Introducing a generalized momentum $\hat{\boldsymbol{p}} \to \hat{\boldsymbol{p}} + e\boldsymbol{A}$ to incorporate such a vector potential leads to the same equations as without a flux tube after the transformation $m \to \tilde{m} = m + f$, namely

$$\left(\partial_r + \tfrac{\tilde{m}+1}{r}\right)\chi_B = (\varepsilon - U(r))\chi_A, \tag{3.29a}$$

$$\left(-\partial_r + \tfrac{\tilde{m}}{r}\right)\chi_A = (\varepsilon - U(r))\chi_B, \tag{3.29b}$$

where the eigenvalue $E = \hbar v_F \varepsilon$ and $V(r) = \hbar v_F U(r)$. Notably, for the non-equivalent second valley the system of Eqs. (3.29) only differs by a permutation of indices A and B,

such that adding the flux does not change any physics compared to the first valley.

3.2.3 Confinement in a quantum well

We shall consider fully-confined zero-modes trapped in the smooth confining potential

$$U(r) = \frac{-U_0}{1 + r^2/d^2}. \tag{3.30}$$

We wish to solve the coupled Eqs. (3.29) by initially finding just the upper radial wavefunction component χ_A. A short-range analysis suggests as $r \to 0$ our solution should be of the form $\chi_A \sim r^{\pm|\tilde{m}|}$; whilst a similar long-range analysis suggests a decay like $\chi_A \sim r^{|\tilde{m}|-p}$ as $r \to \infty$, where

$$p = 1 + |\tilde{m}| + |1 + \tilde{m}|. \tag{3.31}$$

Upon introducing a new variable $\xi = (r/d)^2$, and trying an ansatz solution of the form

$$\chi_A = \xi^{|\tilde{m}|/2}(1 + \xi)^{-p/2} w(\xi), \tag{3.32}$$

where $w(\xi)$ is an unknown function having no bearing on the small or large asymptotics of the solution, we find the following equation for $w(\xi)$

$$\begin{aligned} \xi w'' + \left[1 + |\tilde{m}| + (1 - p)\xi(1 + \xi)^{-1}\right] w' \\ + \tfrac{1}{4}[U_0^2 d^2 (1 + \xi)^{-2} + p^2 \xi (1 + \xi)^{-2} + 2(|\tilde{m}| - \tilde{m} - p|\tilde{m}| - p)(1 + \xi)^{-1}] w = 0. \end{aligned} \tag{3.33}$$

The solution can be given in terms of the Gauss hypergeometric function [79]

$$w(\xi) = {}_2F_1\left(\tfrac{1}{2}[p + U_0 d], \tfrac{1}{2}[p - U_0 d]; 1 + |\tilde{m}|; [1 + \xi^{-1}]^{-1}\right), \tag{3.34}$$

which must be terminated as follows to satisfy the required conditions on its behavior,

$$U_0 d = 2n + p, \quad n = 0, 1, 2... \tag{3.35}$$

The lower radial wavefunction component χ_B is found from χ_A by replacing $\tilde{m} \to -\tilde{m}-1$ and inserting a prefactor of either $U_0 d/2(\tilde{m}+1)$ when $\tilde{m} > 0$ or $2\tilde{m}/U_0 d$ when $\tilde{m} < -1$, whilst the normalization constant is given by

$$C_{\tilde{m},n}^{-2} = \frac{1+\tilde{m}^{-1}}{2} d^2 \int_0^\infty |\chi_A|^2 \mathrm{d}\xi \tag{3.36}$$

where remarkably the integral in Eq. (3.36) can be written in closed form as follows

$$\alpha_n \frac{\Gamma(1+|\tilde{m}|)}{\Gamma(n+p)} \frac{\Gamma(p-|\tilde{m}|+n)}{|1+\tilde{m}|} \left(\prod_{j=1}^{n} (j+|\tilde{m}|) \right)^{-1}, \text{where} \quad \alpha_n = n\alpha_{n-1}, \quad \alpha_0 = 1. \tag{3.37}$$

In the corridor $-1 < \tilde{m} < 0$, we find no valid square-integrable solutions as $r \to \infty$, as whilst $\chi_B \sim r^{-1-|\tilde{m}|}$ when $\tilde{m} \leq -1$, in the regime $\tilde{m} > -1$ we have $\chi_B \sim r^{-|1+\tilde{m}|}$. This corridor is bounded by marginally non-square-integrable states with $\tilde{m} = 0, -1$. Thus the introduction of a flux allows one to have non-vortex like solutions (with quantum numbers $m = 0, -1$) as long as $\tilde{m}$ is not in the corridor of non-square-integrable solutions.

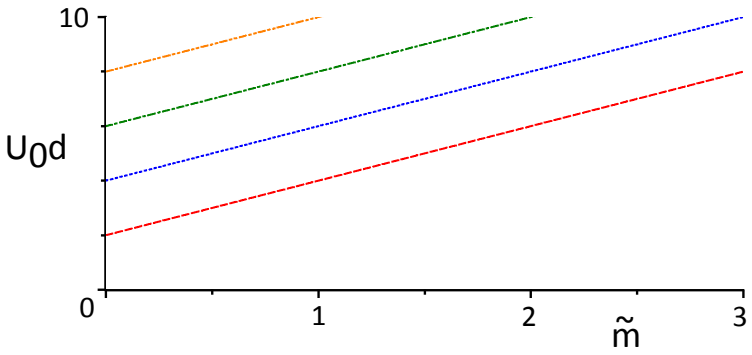

Figure 3.3: Plot of the condition on the scalar potential parameters $U_0 d$ at which the system supports a bound zero-mode, given by Eq. (3.35).

Please note, one needs to also consider the second linearly independent solution of Eqs. (3.29), which has the $r \to 0$ asymptotics $\chi_A \sim r^{-|\tilde{m}|}$, $\chi_B \sim r^{-1-|\tilde{m}|}$ for $-1 < \tilde{m} < 0$. This is similar to the well-known situation with singular anyonic wavefunctions [173]. However, one finds the necessity for square-integrability at infinity removes this solution in this case.

We display Eq. (3.35) graphically in Fig. 3.3. One notices a threshold $U_0 d$ before the first confined mode appears. There is also the usual symmetry about $\tilde{m} \to -\tilde{m} -$

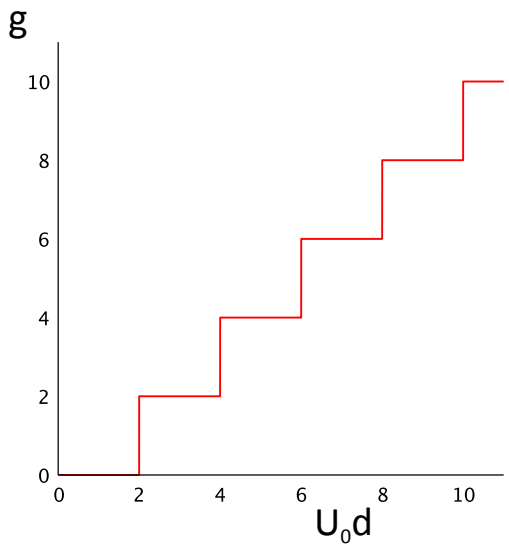

Figure 3.4: Plot of the degeneracy g of each zero mode as a function of potential parameters $U_0 d$.

1. Fig. 3.4 shows the degeneracy g of each fully confined zero-energy state follows an ascending staircase with an increase in the potential parameters $U_0 d$. It can be envisaged that such few particle quantum dots will be naturally favored due to screening effects supporting the tendency of the system to minimize the total energy.

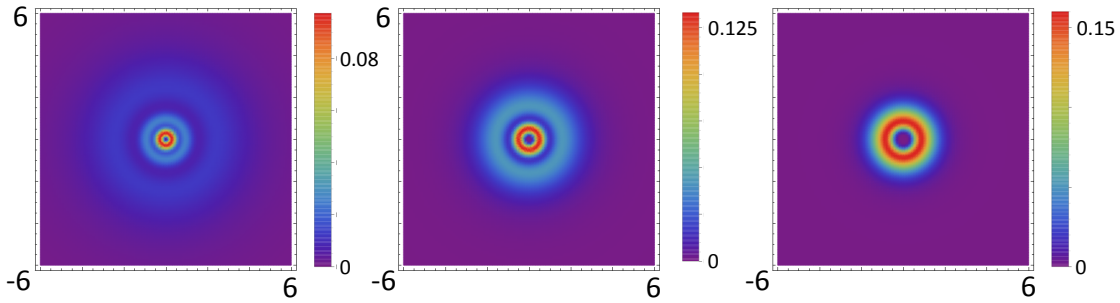

Figure 3.5: Plot of density $|\Psi|^2 d^2$ as a function of distance measured in units of d, for a dot with $U_0 d = 8$ and (left-to-right) parameters $(\tilde{m}, n) = (1, 2), (2, 1)$ and $(3, 0)$.

We show in Fig. 3.5 how a modulation of $\tilde{m}$ can lead to different states $(\tilde{m}, n)$ in a dot held at a constant $U_0 d$. One can see the ring-like structure of electron density for all states, necessary to avoid Klein tunneling, and how increasing $\tilde{m}$ gives rise to increasingly tight confined states, as expected from the asymptotic form of the wavefunction as $r \to \infty$. Notably, unlike the square-well toy model, one does not need to introduce a regularization scheme for the vector potential[169], rather they are true quantum mechanical solutions.

3.2.4 Confinement in a quantum ring

There is a continued interest in quantum rings [174] due to the range of exotic physical effects that can be observed in such non-simply connected nanostructures [175, 176, 177]. For our particular interest of zero-energy states in a magnetic flux, we find a similar situation occurs in the case of a ring-like confining potential as for a potential well, for example consider

$$U(r) = U_0\Theta(r-a)\Theta(b-r), \tag{3.38}$$

where $b > a$ defines the width of the ring. Bound states do not occur in the window $-1 < \tilde{m} < 0$, but outside can exist when the following eigenvalue condition is satisfied, for $\tilde{m} > 0$

$$J_{|\tilde{m}|}(U_0a)Y_{|\tilde{m}+1|}(U_0b) = J_{|\tilde{m}+1|}(U_0b)Y_{|\tilde{m}|}(U_0a), \tag{3.39}$$

whilst for $\tilde{m} < -1$ the required equation is found upon making the replacements $a \to b$ and $b \to a$ everywhere; both transcendental equations can be solved by usual root-finding methods and a typical result is given in Fig. 3.6. Again, a threshold U_0b is seen below which no bound states are supported.

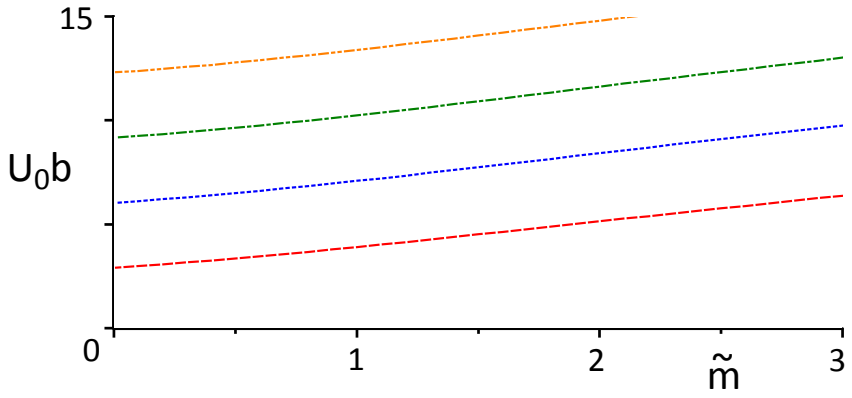

Figure 3.6: Plot of the condition on the scalar potential parameters U_0b at which the system supports a bound zero-mode, given by Eq. (3.39) for $U_0a = 1$.

A characteristic plot of the two lowest electron densities is shown in Fig. 3.7 for $U_0b = 7$ and $U_0a = 1$. It is seen an increase in $\tilde{m}$, and so flux, brings about successively higher states, distinguished by an increasing numbers of peaks, at specific values of U_0b for a set U_0a.

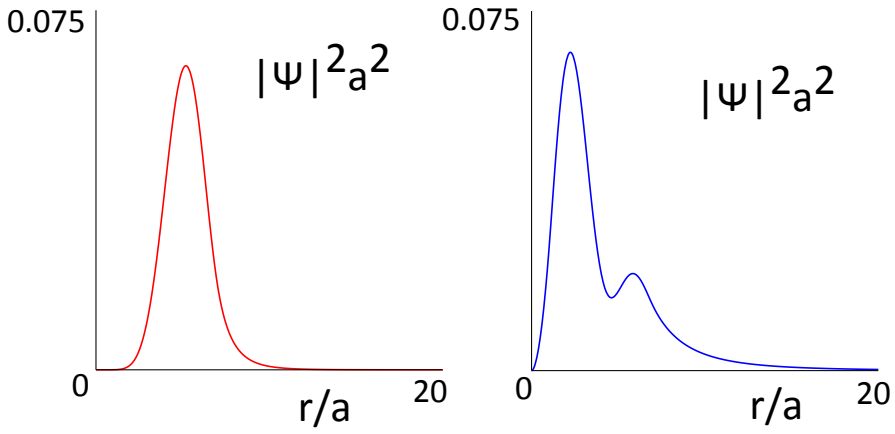

Figure 3.7: Plot of the electron densities of the two modes supported in a ring defined by $U_0 b = 7$ and $U_0 a = 1$, such that (left) $\tilde{m} = 3.51$ and (right) $\tilde{m} = 0.932$.

3.2.5 Conclusion

We have suggested that the system of zero modes of the Dirac equation in an electrostatically-defined quantum dot or ring, realizable in graphene, can be manipulated with the help of a magnetic flux to bring about confinement and deconfinement.

The proposed effect of magnetic deconfinement of electrostatically trapped states in graphene has important potential applications. Indeed, an ability to modify the free carrier density by weak external magnetic fields in conjunction with graphene's superior transport properties can be utilized in novel magnetic read out devices [178, 179].

3.3 Optimal electrostatic traps

We transform the two-dimensional Dirac-Weyl equation, which governs the charge carriers in graphene, into a non-linear first-order differential equation for scattering phase shift, using the so-called variable phase method. This allows us to utilize the Levinson Theorem to find zero-energy bound states created electrostatically in realistic structures. These confined states are formed at critical potential strengths, which leads to us posit the use of 'optimal traps' to combat the chiral tunneling found in graphene, which could be explored experimentally with an artificial network of point charges held above the graphene layer. We also discuss scattering on these states and find the $m = 0$ states creates a dominant peak in scattering cross-section as energy tends towards the Dirac point energy, suggesting a dominant contribution to resistivity.

3.3.1 Introduction

The electronic properties of the two-dimensional (2-D) material graphene [180, 181] are of great interest due to the quasi-relativistic nature of its spectrum. Interesting transport effects such as chiral (Klein) tunneling [9, 31, 150, 151, 182], vacuum polarization [55], atomic collapse [56, 183] and the minimum conductivity at the Dirac point [124] have been widely discussed in the literature. The topic of elastic scattering in clean, low-temperature graphene, which can occur due to charged impurities, ripples or strain fields, has been addressed by many authors [184, 185, 186].

However, despite its extraordinary properties there is a major obstacle stopping graphene from usurping silicon in the electronics industry, namely is its lack of a bandgap. This frustrates attempts to perform digital logic with graphene due to the difficulty in turning off the chiral charge carriers which always wish to conduct. Attempts at opening a gap in monolayer graphene have focused on chemical functionalization [187] and strain engineering [188], which can unfortunately blunt the remarkable electronic properties which makes graphene so attractive. Here we propose a method not to open a gap, but to switch off the chiral tunneling by considering zero-energy states, when the Fermi energy coincides with the Dirac points, such that fully confined states are predicted to be able to form due to the absence of pseudospin [68, 160]. In fact, these states are the most

important factor when considering resonant scattering in graphene.

Despite the appearance of sophisticated experimental techniques for probing resonances and the modification of the density of states in the continuum [189] the search for fully-confined (square-integrable) states remains a significant ongoing task. Efficient manipulation of the Fermi level requires the presence of a back-gate in close proximity to the graphene, which makes the numerous beautiful results stemming from the long-range behavior of the bare Coulomb potential [56] to be somewhat far from experimental reality, as the presence of image charges in the gate material (or screening effects) make any realistic potential fall at large distances faster than $1/r$. However, it is well known that any fast-decaying potential cannot produce a bound state at nonzero energy [90]. Indeed, the asymptotic of the wavefunction is a Bessel function decaying asymptotically only like $r^{-1/2}$, and so one is led to consider zero-energy states instead.

Whilst low-energy resonant scattering in monolayer graphene has been intensively studied by previous authors both theoretically [56, 90, 190, 191, 192, 193, 194, 195, 196, 197, 198] and experimentally [199, 200, 201, 202] the importance of fully-confined zero-energy states in realistic structures has not been fully appreciated until recently [161]. Thus far, only quasi-bound states, where only one wavefunction component is confined or when the wavefunction is non-square integrable, have been considered for resonant scattering. Previously, only circular wells [90, 191] or the Coulomb potential [55, 192], have been investigated, but here we concentrate on smooth [203], short-range potentials which are defined by two parameters, characterizing both strength and spread.

We study confined states and resonant scattering in graphene due to either scanning probe microscopy (SPM) [204] tip-induced potentials or due to some charge displaced out of the plane [205], with careful consideration of truly bound zero-modes. The strength parameter can arise due to, for example, the size of the charge on the SPM, whilst the spread parameter is linked to the distance from the SPM tip to the graphene. We investigate both the conditions required for a zero-energy bound state to form and the effect of such states in our study on the energy dependence of scattering cross-section and resistivity contributions of resonant scatterers. We also note there is increasing interest in zero-modes of the Dirac equation in the condensed matter community due to the possibilities of both

observing the elusive Majorana fermions [163] or indeed fractionally charged excitations [162].

To carry out our investigations into realistic, short-range (due to the necessity of a gate in all measurements) potentials we develop the variable phase method or VPM [206, 207], which was found to be useful for tackling scattering problems governed by the Schrödinger equation in 2-D [208, 209, 210, 211], for use with the 2-D Dirac-Weyl equation - allowing us to consider the charge carriers of graphene. The VPM was originally developed [212] for use with non-relativistic wave equations in the 1930s as a neat tool to calculate physically relevant quantities directly, rather than having to extract them from the wavefunction, and has recently been developed for use with the Dirac-Weyl equation in quasi-one-dimensional problems due to the intense interest in graphene in the condensed matter community [213]. Here we derive a first-order equation from which we can immediately find the scattering phase shift. This is advantageous as important physical properties directly follow, such as: the number of bound states (from the Levinson Theorem) [214]; the scattering and transport cross-sections (from standard elastic scattering theory) [215]; the number of states around a potential barrier (using the Friedel sum rule) [216]; and the energy change due to the impurity interacting with neighboring electrons (the Fumi theorem) [217]. We have neglected effects due to rippling of or dislocations in the graphene membrane. We also do not discuss scattering by multiple electrostatic barriers or by magnetic barriers [139, 218, 219], but our method can be generalized to account for the presence of vector potentials.

3.3.2 Formalism of the variable phase method

The 2-D Dirac-Weyl Hamiltonian governing the low-energy charge carriers of graphene on Dirac cones is [181]

$$\hat{H} = v_{\mathrm{F}}\boldsymbol{\sigma}\cdot\hat{\boldsymbol{p}} + U(r) + \sigma_z\Lambda, \tag{3.40}$$

where $v_{\mathrm{F}} \approx c/300$ is the Fermi velocity of the Dirac particles, $\boldsymbol{\sigma} = (\sigma_x, \sigma_y, \sigma_z)$ are the Pauli spin matrices, $U(r)$ is a central potential and Λ is the mass term. A non-zero mass can arise due to chemical modifications or by strain engineering [127]. We move into polar coordinates (r, θ) for circular symmetry, and separate the variables via the following

ansatz for the two-component spinor wavefunction

$$\Psi(r,\theta) = \frac{e^{im\theta}}{\sqrt{2\pi}} \begin{pmatrix} \chi_A(r) \\ ie^{i\theta}\chi_B(r) \end{pmatrix}, \qquad m = 0, \pm 1, \pm 2, ... \tag{3.41}$$

where the subscripts A and B label the two sublattices of the graphene chicken wire lattice. This choice of wavefunction leads to two coupled first-order differential equations for the radial wavefunction components $\chi_{A,B}(r)$

$$\left(\frac{d}{dr} + \frac{m+1}{r}\right)\chi_B = (k - V(r) - \Delta)\chi_A, \tag{3.42a}$$

$$\left(-\frac{d}{dr} + \frac{m}{r}\right)\chi_A = (k - V(r) + \Delta)\chi_B, \tag{3.42b}$$

with $V(r) = U(r)/\hbar v_\mathrm{F}$, $\Delta = \Lambda/\hbar v_\mathrm{F}$ and $k = E/\hbar v_\mathrm{F}$, where E is the eigenenergy. Rearranging Eqs. (3.42) into a second-order differential equation for a single radial wavefunction component $\chi_A(r)$ we obtain for the massless case

$$\frac{d^2}{dr^2}\chi_A(r) + \left(\frac{1}{r} + \frac{1}{k - V(r)}\frac{dV(r)}{dr}\right)\frac{d}{dr}\chi_A(r) + \left((k - V(r))^2 - \frac{m}{r}\frac{1}{k - V(r)}\frac{dV(r)}{dr} - \frac{m^2}{r^2}\right)\chi_A(r) = 0. \tag{3.43}$$

We consider potentials of the form $V(r \to \infty) = 0$ such that at large distances Eq. (3.43) reduces to

$$\frac{d^2}{dr^2}\chi_A(r) + \left(\frac{1}{r}\right)\frac{d}{dr}\chi_A(r) + \left(k^2 - \frac{m^2}{r^2}\right)\chi_A(r) = 0, \tag{3.44}$$

this condition prohibits potentials decaying slower than r^{-2} as $r \to \infty$. Otherwise the asymptotic solution of Eq. (3.43) always adds to the phase shift however large r becomes, as is familiar from the asymptotic behavior of the Coulomb wavefunction in the non-relativistic case. Eq. (3.44) is a form of the Bessel equation with the well-known solution $a_m J_m(kr) + b_m N_m(kr)$, or equivalently

$$\chi_A(r) = A_m \left[J_m(kr)\cos(\delta_m) - N_m(kr)\sin(\delta_m)\right], \tag{3.45}$$

where $J_m(kr)$ and $N_m(kr)$ are the Bessel functions of the first and second kinds respectively, and $\delta_m = \arctan(-\frac{b_m}{a_m})$ is the scattering phase shift, arising from the difference in phase of the wavefunction at $r \to \infty$ compared to the free particle case.

We now implement the VPM by treating the constants A_m and δ_m as functions of the radial coordinate r, such that

$$\chi_A(r) = A_m(r)\left[J_m(kr)\cos(\delta_m(r)) - N_m(kr)\sin(\delta_m(r))\right], \tag{3.46}$$

where $A_m(r)$ is called the amplitude function and the phase function δ_m is the phase shift arising from a potential cut-off at a distance r. To completely define these newly introduced functions $A_m(r)$ and δ_m we make the following ansatz for the first derivative of $\chi_A(r)$ with respect to r

$$\chi'_A(r) = A_m(r)\left[J'_m(kr)\cos(\delta_m(r)) - N'_m(kr)\sin(\delta_m(r))\right], \tag{3.47}$$

where $'$ denotes differentiation with respect to r. Now, setting the direct derivative of Eq. (3.46) equal to Eq. (3.47) suggests the following useful condition

$$\frac{A'_m(r)}{A_m(r)} = \delta'_m(r)\frac{J_m(kr)\sin(\delta_m(r)) + N_m(kr)\cos(\delta_m(r))}{J_m(kr)\cos(\delta_m(r)) - N_m(kr)\sin(\delta_m(r))}. \tag{3.48}$$

Upon substituting Eq. (3.46) and Eq. (3.47) into the lower coupled Eq. (3.42b) we naturally find the lower radial wavefunction component $\chi_B(r)$ is

$$\chi_B(r) = \frac{A_m(r)}{k - V(r)}\left[\left(-J'_m(kr) + \frac{m}{r}J_m(kr)\right)\cos(\delta_m(r)) - \left(-N'_m(kr) + \frac{m}{r}N_m(kr)\right)\sin(\delta_m(r))\right]. \tag{3.49}$$

We can now utilize the upper coupled Eq. (3.42a): upon substituting in Eq. (3.45) and Eq. (3.49) and eliminating the amplitude function $A_m(r)$ via the application of the condi-

tion Eq. (3.48), we obtain the following first-order differential equation

$$\begin{aligned}\frac{d}{dr}\delta_m(r) = \frac{\pi r}{2}p(r)\left[\frac{1}{k-V(r)}\frac{dV(r)}{dr}\left(q(r)-\frac{m}{r}p(r)\right)+\left(V(r)^2-2kV(r)\right)p(r)\right],\\ p(r) = J_m(kr)\cos(\delta_m(r)) - N_m(kr)\sin(\delta_m(r)),\\ q(r) = J'_m(kr)\cos(\delta_m(r)) - N'_m(kr)\sin(\delta_m(r)),\end{aligned} \tag{3.50}$$

where we have introduced the auxiliary functions $p(r)$ and $q(r)$ and in addition have used the Wronskian of the Bessel functions $W\{J_m(x), N_m(x)\} = J_m(x)N'_m(x) - N_m(x)J'_m(x) = -\frac{2}{\pi x}$ to simplify the final expression [220]. Eq. (3.50) is the so-called phase equation, and is subject to the initial condition $\delta_m(0) = 0$, as follows from being in the free particle limit. We can see from Eq. (3.50) how the potential $V(r)$ gradually accumulates the desired phase shift starting from $\delta_m(0) = 0$ and finishing with the total phase shift of the scattering problem, given by

$$\delta_m = \lim_{r\to\infty}\delta_m(r). \tag{3.51}$$

This condition ensures the phase shift is uniquely defined, avoiding an ambiguity of π that appears in other methods [215].

When considering bound states in the massless case we can only consider zero-energy states, where the Neumann function is divergent and so the following condition is implied to guarantee that $sin\,(\delta_m) = 0$ in Eq. (3.50)

$$\delta_m = n\pi, \qquad n = 1, 2, 3... \tag{3.52}$$

Eq. (3.52) is related to the Levinson's theorem for massless Dirac particles, which states a relation between the phase shift at zero-momentum and the number of bound states.

Please note when considering the celebrated massive Dirac particles, e.g. found in h-BN or gapped graphene [221], which allow bound states at finite energy, an equation

analogous to the phase equation Eq. (3.52) can be derived for treating confined states

$$\begin{aligned}\frac{d}{dr}\eta_m(r) = -rf(r)\left[\frac{1}{k-V(r)}\frac{dV(r)}{dr}\left(g(r)-\frac{m}{r}f(r)\right)+\left(V(r)^2-2kV(r)\right)f(r)\right],\\ f(r) = I_m(\kappa r)\cos(\eta_m(r)) - K_m(\kappa r)\sin(\eta_m(r)),\\ g(r) = I'_m(\kappa r)\cos(\eta_m(r)) - K'_m(\kappa r)\sin(\eta_m(r)),\end{aligned} \tag{3.53}$$

where $I_m(\kappa r)$ and $K_m(\kappa r)$ are the modified Bessel and Neumann functions respectively and the effective wavevector $\kappa = (\Delta^2 - k^2)^{1/2}$. Eq. (3.53) has been simplified [220] by noting the Wronskian of the modified Bessel functions $W\{I_m(x), K_m(x)\} = I_m(x)K'_m(x) - K_m(x)I'_m(x) = -\frac{1}{x}$. Notably, Eq. (3.53) is also relevant for considerations of the surface states on 3-D topological insulators such as Bi_2Te_3, where in this case the mass term arises from the exchange energy from a magnetic insulator [222]. When considering bound states we note the modified Bessel function of the first kind is divergent and so the following condition is implied so that $\cos(\delta_m) = 0$ in Eq. (3.53)

$$\eta_m = \left(n - \frac{1}{2}\right)\pi, \qquad n = 1, 2, 3... \tag{3.54}$$

Eq. (3.54) is connected to the Levinson's theorem for the massive Dirac equation [223, 224].

3.3.3 Influence on scattering

We now check we can reproduce known results by solving the phase equation Eq. (3.51), describing the massless charge carriers of graphene, for the case of zero-energy states formed in a Lorentzian potential $V(r) = -V_0/(1 + (r/d)^2)$, an analytically solved problem [225]. In this case the condition for bound states when $m \geq 0$ is $(V_0 d)_{N,m} = 2(N + m)$, where $N = 1, 2, 3...$ is a positive integer. Thus when solving Eq. (3.51), the phase equation for massless Dirac particles, when $k \to 0$ we should see the threshold value of $V_0 d$ met before step-like behavior as $V_0 d$ is turned up and more confined zero-energy states appear. This is exactly what we find in Fig. 3.8 (top). We also note the sign of V_0 is irrelevant for the creation of zero-energy confined states as a well for electron is a hill for a hole and vice versa, thus Fig. 3.8 has mirror symmetry about the δ_m axis. At the Dirac point, when

the density of states vanishes yet the conductivity remains finite, these zero-energy states should be important as we shall see later on.

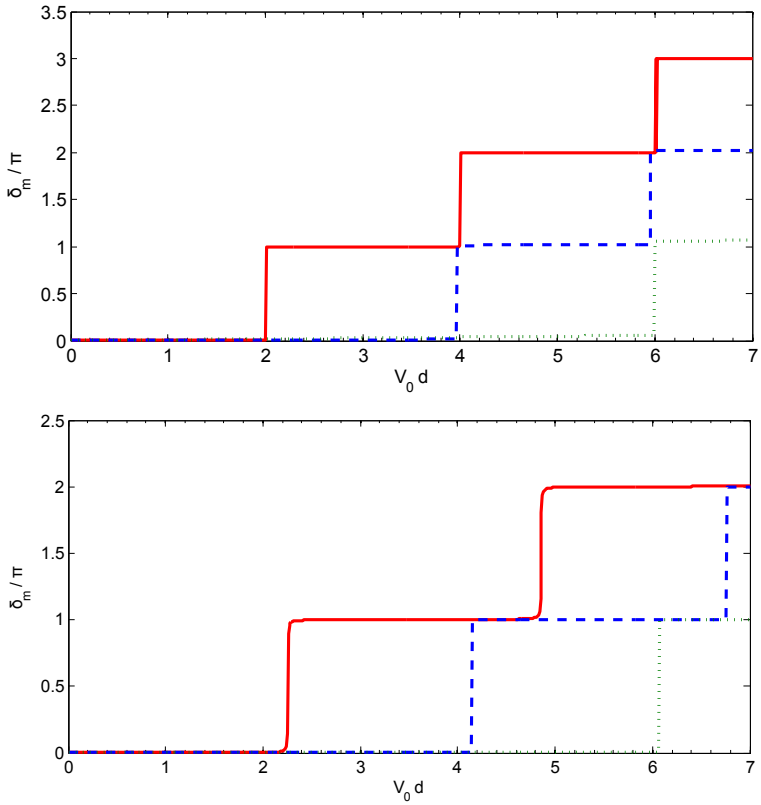

Figure 3.8: Plots of scaled phase shift δ_m/π against potential strength $V_0 d$ for massless Dirac particles, of energy tending towards zero, incident on (top) the Lorentzian potential and (bottom) the model potential of Eq. (3.55) with the realistic $1/r^3$ decay. We show results for angular momentum $m = 0, 1, 2$ corresponding to the solid line (red), dashed line (blue) and dotted line (green) respectively.

Whilst screening only affects the strength of the Coulomb potential and not its characteristic decay [186], due to the quasi-relativistic nature of the carriers in graphene, a cut-off is necessary at the origin and the presence of an image charge necessarily in the substrate will lead to a dipole-like $1/r^3$ decay at large distances, thus a convenient choice of model potential is

$$V(r) = \frac{-V_0}{1 + (r/d)^3}. \tag{3.55}$$

In Fig. 3.8 (bottom) we investigate confined states with Eq. (3.55) and again see a characteristic threshold potential strength product spread $V_0 d$, followed by the signature staircase behavior of confined zero-energy states. Of course, compared to the exactly-solvable

Lorentzian potential with its accidental degeneracies, the staircase does not share the same beautiful symmetries and the condition for full-confined states can be approximated by $(V_0 d)_{N,m} \approx 2.63N + 1.89m - 0.34$. However we can now predict in realistic graphene flakes, where we would expect charged impurities to cause potentials similar to the type of Eq. (3.55), there is the possibility for the appearance of fully-confined zero-energy states.

Experimentally, such states should be able to be detected by SPM experiments, as previously proposed [225], where smoothly changing either the charge on the SPM tips or their distance above the graphene plane, and continuously holding the Fermi level at the Dirac point using the back-gate should be sufficient to see confined zero-modes. A network of SPM tips, of radius R_{tip} and separated in a square grid defined by a distance s, held at a distance h_2 above a metallic back gate and $h_2 - h_1$ above the graphene plane gives a similarly behaved potential to Eq. (3.55), but in a more complicated form due to the method of images,

$$U(r) = \frac{eQ_{tip}}{4\pi\epsilon_0\epsilon_r} f(r),$$
$$f(r) = \sum_{j,k=-n_1}^{n_2} \left((x+js)^2 + (y+ks)^2 + (h_2-h_1)^2\right)^{-1/2} - \left((x+js)^2 + (y+ks)^2 + (h_2+h_1)^2\right)^{-1/2}. \tag{3.56}$$

Fitting Eq. (3.55) to Eq. (3.56) by matching the functions at both their maximum and half-maximum values, one finds that the tip voltage V_{tip} at which one would see such zero-modes is

$$V_{tip} = \frac{(V_0 d)_{N,m}}{f(0)d} \frac{\hbar v_F}{eR_{tip}}, \quad \text{subject to the constraint } 2f(d) = f(0), \tag{3.57}$$

where we have seen from Fig. 3.8 (bottom) the dimensionless parameter $(V_0 d)_{N,m\neq 0} = 4.16, 6.06, 6.79...$ such that we are dealing with tip voltages of the order of tens of mV, $V_{tip} = 20\text{mV}, 29\text{mV}, 33\text{mV}$ and so on. (In this estimate, we use $h_2 = 300\text{nm}$, $h_1 = 200\text{nm}$, $s = 40\text{nm}$, $R = 5\text{nm}$ and $n_1 = n_2 = 2$). The existence of confined states opens up the possibility of Coulomb blockade-type physics in graphene. Indeed, the quantum dots

created with careful adjustment of the key parameters can be be seen to be 'optimal traps'. An estimate of the charging energy of the optimal trap, using a simple disc capacitor model, shows a charging energy of the order of meV, thus such effects could be seen at room temperature. The effect arises due to the tightly confined nature of the wavefunction in optimal traps which leads to small capacitance and a significant charging energy, which is negligible for the usual deconfined states.

We also show in Fig. 3.9 that the zero-modes of the Dirac equation in the potential Eq. (3.55), as predicted in the continuum model, are indeed present as shown via tight-binding calculations [226, 227]. It is found the wavefunctions have a ring-like structure, which ensures avoidance of any Klein tunneling effects, i.e the states are zero-energy vortices with $m \neq 0$. It is most noticeable how by adjusting the parameter $V_0 d$ one can go from a tightly confined state to a state with a highly spread probability density. We have also checked the zero-modes are robust to the shape of the graphene flake by investigating triangle and hexagon geometries, with both zig-zag and armchair boundaries.

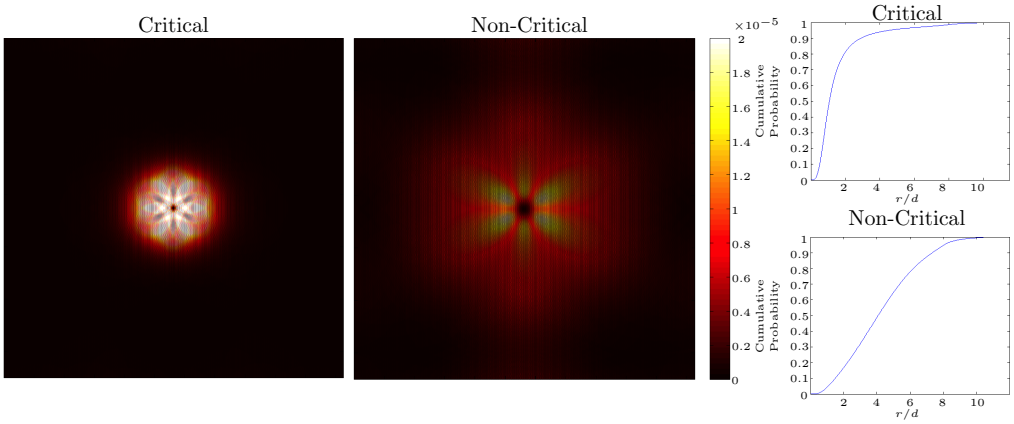

Figure 3.9: Probability density plots of near zero-energy states confined within the model confining potential Eq. (3.55), as calculated via tight-binding methods. We show example critical $V_0 d = 4.10$ (left) and non-critical $V_0 d = 2.60$ (right) states, as well as the associated cumulative probability plots (right).

As mentioned previously, once the scattering phase shift is known a number of other useful physical properties can be quickly calculated. The partial cross-section ζ_m can be taken as

$$k\zeta_m = \sin^2(\delta_m), \tag{3.58}$$

whilst the total scattering cross-section ζ, a measure of the one-dimensional area felt by

oncoming particles, and the transport cross-section ζ_T easily follow from the scattering phase shifts via

$$\zeta = \frac{4}{k}\sum_{m=-\infty}^{\infty}\sin^2(\delta_m), \quad \zeta_T = \frac{2}{k}\sum_{m=-\infty}^{\infty}\sin^2(\delta_{m+1}-\delta_m), \tag{3.59}$$

and we note for low-energy scattering we can take the s-wave approximation, i.e. only small m need to be considered as Eq. (3.58) is derived from partial-wave expansions where terms with high m are negligible when $k \to 0$. Detailed derivations of Eq. (3.58) and Eq. (3.59) via 2D elastic scattering theory adapted for Dirac fermions have been given by Novikov [192].

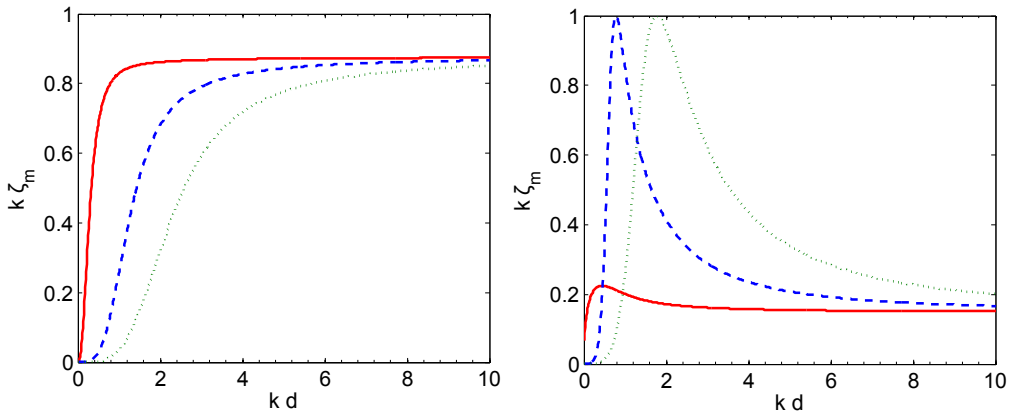

Figure 3.10: A plot of dimensionless partial scattering cross-section $k\zeta_m$ as a function of scaled energy k for massless Dirac particles incident on the model potential with $1/r^3$ decay given by Eq. (3.55), with example noncritical potential strength (left) $V_0 d = 1.00$ and critical (right) $(V_0 d)_{1,0} = 2.27$. We show results for $m = 0, 1, 2$, corresponding to the solid line (red), dashed line (blue) and dotted line (green) respectively.

The energy dependence of scattering cross-section has previously been considered for a square well [90, 191]. We will now revisit the problem with a smooth, short-range potential given by Eq. (3.55), which is relevant for gated structures or for hypercritical charges. We show in Fig. 3.10 plots of dimensionless partial cross-section $k\zeta_m$ for the case of non-critical (left) and critical (right) parameters of the potential Eq. (3.55). We find, in contrast to the general case, at the critical potential strength the $m = 0$ non-square-integrable state does not go to zero in $k\zeta_m$ as quickly as k tends towards zero, and thus is divergent in partial cross-section ζ_m as energy tends towards zero. This is because $m = 0$ is

a resonant state with a non-normalizable wavefunction (and a non-zero probability density at the origin $r = 0$) and so such a particle has an enhanced likelihood of being scattered. Of course, this behavior remains in calculations of transport scattering cross-section via Eq. (3.59).

We also note, in striking contrast to non-relativistic particles, at large energies the phase shift δ_∞ is non-zero [228]. Remarkably, δ_∞ is also angular momentum-independent and we find from Eq. (3.51) the explicit form

$$\delta_\infty = -\int_0^\infty V(r)\mathrm{d}r, \tag{3.60}$$

such that for the considered potential Eq. (3.56) the dimensionless partial scattering cross-section in the large energy limit is given by $k\zeta_m \to \sin^2(\frac{2\pi}{3\sqrt{3}}V_0 d)$, as displayed in Fig. 3.10. Thus, the transport cross-section ζ_T vanishes in this limit.

The smoking gun of confined zero-modes in the laboratory could be via their contribution to resistivity, which in semiclassical Boltzmann theory can be expressed as [191]

$$\rho = \frac{h}{4e^2}\frac{2n_s}{\pi n_e}k\zeta_T \tag{3.61}$$

where n_s is the density of scatterers and the electron density $n_e = k^2/\pi$. We show in Fig. 3.11 the behavior of resistivity at small kd. The presence of confined zero-modes leads to a divergence in resistivity at energies tending towards zero in the critical case only, $\rho[h/4e^2] \to \infty$. It should be possible to utilize this consequent drastic suppression of mobility to create an off-state in graphene, perhaps this can be explored artificially with a series of point gates held above the graphene monolayer. In the non-critical cases, we find as $k \to 0$ resistivity saturates to a constant.

3.3.4 Conclusion

We have derived the phase equations for the 2-D Dirac equation using the VPM, suitable for use straightaway in scattering calculations concerning graphene. In doing so, we provide a numerical (experimental) proof of the Levinson Theorem for massless 2-D particles. These phase equations are of first-order, and so relatively undemanding compu-

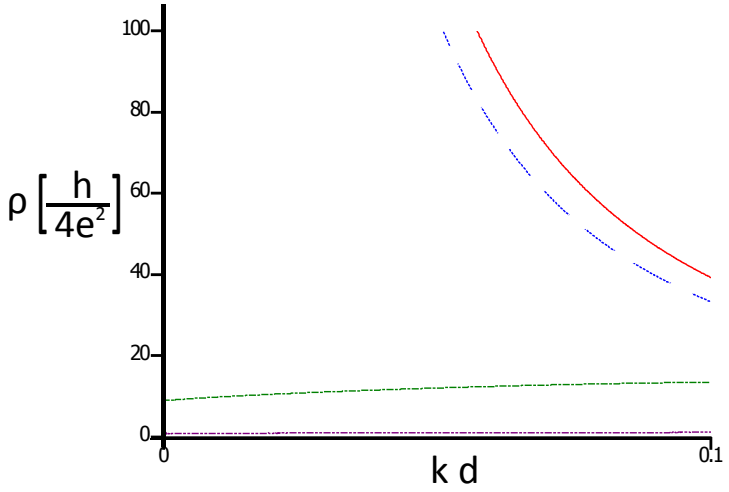

Figure 3.11: A plot of resistivity ρ, measured in units of $h/4e^2$, as a function of energy kd for massless Dirac particles scattering on the model potential with $1/r^3$ decay. We show results for example uncritical cases $V_0 d = 1.00, 3.00$, corresponding to the dash-dot line (green) and dash-dot-dot line (purple) respectively, and example critical cases $V_0 d = 2.27, 4.87$, corresponding to the solid line (red) and dashed line (blue) respectively. We set $2n_s d^2 = 1$.

tationally, and have solutions in terms of scattering phase shifts, thus other desired scattering properties readily follow. Applying the method to fully-confined states in graphene, we reproduce an exact result from the literature and go on to investigate a more physical potential again finding that a certain potential strengths and spreads zero-energy bound states are likely to form, which is most important when describing resonant scattering.

We have also calculated the energy dependence of scattering cross-section, finding a major distinction for the $m = 0$ mode for critical potential strengths (those able to support truly bound states). In this special case, we predict a dominant peak in scattering cross-section at zero-energy, suggesting a high probability of being scattered, which can be explored experimentally via scanning probe microscopy. In an experiment with a series of point gates above the graphene layer, one may be able to use artificial resonant scattering to switch off the chiral tunneling effect found in monolayer graphene by greatly reducing the mobility of carriers.

3.4 Pair states in gapless graphene

We study the formation of bound two-particle states, either excitons or bi-electronic pairs, in gapless monolayer graphene in gated structures. We find that, even in the regime of massless Dirac particles, coupling can occur at zero-energy. We propose the possibility of a condensate of such excitons, and suggest a new picture of the experimentally seen Fermi velocity renormalization.

3.4.1 Introduction

The two-dimensional allotrope of carbon graphene continues to attract attention in the condensed matter community, and a particular current focus is in creating exotic heterostructures [229, 230]. Recently, some remarkable Coulomb drag experiments have been performed on spatially separated graphene systems [231, 232], where it has been shown there is a giant magnetodrag at the charge neutrality point. Additionally, several recent theoretical treatments have been proposed to explain this phenomena [233, 234, 235, 236, 237]. Theoretical works prior to the groundbreaking experiments have posited fascinating effects, such as a ghost excitonic insulator transition [238], non-Fermi liquid behavior [239, 240], and metal-insulator phase transitions [241, 242]. Importantly in such spatially separated graphene systems, there is a hope to find a so-called interlayer exciton, comprised of a stable bound state between an electron and a hole in different layers [243]. This raises the prospect of soon seeing an exciton condensate of Dirac particles in the laboratory.

Previous theoretical works on excitonic effects in Dirac materials have approached the problem in either a Bethe-Salpeter formalism [244] or in the language of a two-body matrix Hamiltonian [69]. It has been shown there is a nontrivial coupling between the center-of-mass and the relative coordinates in the quasi-relativistic two-body problem, and the special case of zero total momentum of the pair has been mostly considered [245, 246]. Indeed, it claimed excitons do not exist in gapless graphene [247] but considerations of trigonal warping have been suggested as a route towards excitonic formation [248, 249]. However no gap has as yet been observed experimentally [250] and a question remains: can excitons exist in gapless graphene? We should mention with the help of a gap, Berman

and co-workers have studied Bose-Einstein condensation in bilayer graphene [251] and superfluidity [252, 253] and condensation [254] in two-layer graphene. Additionally, Lozovik and co-workers have studied the superconducting pairing of electrons due to phonons [255, 256, 257].

Whilst in quasi-one dimensional Dirac materials, bound states do appear, we note truly (square-integrable) bound states occur only at zero-energy for Dirac particles in the single particle picture in a radial scalar potential [160, 258]. Mathematically, this is because at finite energy the effective Schrodinger equation at long range maps on to the problem of scattering states in a non-relativistic system (with solutions decaying like the square root of distance); whereas at zero energy solutions exist which decay algebraically (depending on the angular momentum quantum number m). When m is nonzero the solutions are fully square-integrable, such that they are rotating ring-like states, which always avoid the Klein tunneling due to their vorticity resulting in a nonzero momentum component along the potential barrier. In this work, we show via an exact solution of the quasi-relativistic two-body problem zero-energy pairs can occur in gapless graphene, as long as they are rotating vortices with nonzero angular momentum $m \neq 0, -1$.

As only states with nonzero angular momentum are square-integrable, one should not be able to find bound states with a nonzero center-of-mass momentum K. In this circumstance angular momentum is not a good quantum number and so one must construct solutions as a series expansion over all momenta, which will include the zero angular momentum state which acts to deconfine the whole state and hence will not correspond to a truly bound solution. Then it is natural to conclude one can only condense the excitons in the zero-energy state at $K = 0$, they are pinned vortex pairs.

An important feature of this system is the fact that the zero-mode eigenvalue spectrum will be insensitive to the sign of the interaction $U(r)$ as it only appears as a logarithmic derivative or squared. Therefore as well as standard excitons there is the possibility to obtain somewhat exotic bi-electronic (electron-electron) pairs.

It is important to consider gated structures, which modifies the situation from a pure Coulomb problem [55, 56]. The necessity for metallic gates inevitably leads to image charges which leads to short-range interactions [205, 259] and an Ohno-type cutoff

as is known in studies of polymer systems [64]. Of course, in this setup the dielectric environment is still of great importance [260], as is the geometry of the device which both contribute to the effective strength of the interaction.

The necessity for pairing at zero-energy leads to the requirement of a fine-tuning of the interaction strength to support an excitonic state that can be naturally achieved in the system via screening.

3.4.2 A proposal to pair electrons

The two-body Hamiltonian can be written as the Kronecker sum of the single-particle Hamiltonians $H = H_1 \oplus H_2$, or explicitly (as there are two sublattices and two particles) as the 4×4 matrix

$$H = v_F \begin{bmatrix} 0 & p_{x_2} - ip_{y_2} & -p_{x_1} + ip_{y_1} & 0 \\ p_{x_2} + ip_{y_2} & 0 & 0 & -p_{x_1} + ip_{y_1} \\ -p_{x_1} - ip_{y_1} & 0 & 0 & p_{x_2} - ip_{y_2} \\ 0 & -p_{x_1} - ip_{y_1} & p_{x_2} + ip_{y_2} & 0 \end{bmatrix}, \tag{3.62}$$

where the subscripts 1 and 2 refer to the two particles. The Hamiltonian acts upon a two-particle wavefunction constructed via the Kronecker product $\Psi(\mathbf{r}_1, \mathbf{r}_2) = \psi_i(\mathbf{r}_1) \otimes \psi_j(\mathbf{r}_2)$, where $i, j = (A, B)$. In the absence of an interaction potential $\mathcal{I}U(r)$, we find upon diagonalization of Eq. (3.62) four eigenenergies:

$$E = \pm v_F \left(p_{x_1}^2 + p_{y_1}^2\right)^{1/2} \pm v_F \left(p_{x_2}^2 + p_{y_2}^2\right)^{1/2}. \tag{3.63}$$

As is usual with two-body problems, utilizing center of mass and relative motion coordinates: $X = (x_1 + x_2)/2$, $Y = (y_1 + y_2)/2$, $x = x_1 - x_2$, $y = y_1 - y_2$; and assuming a translationally-invariant system such that the center-of-mass momentum $\hbar\boldsymbol{K}$ is a constant of motion, one can employ the ansatz $\Psi_i(\boldsymbol{R}, \boldsymbol{r}) = \exp(i\boldsymbol{K} \cdot \boldsymbol{R})\psi_i(\mathbf{r})$, where $i = (1, 2, 3, 4)$ builds the four component wavefunction components via the two sublattices and two particle species. Now the eigenenergies are redefined via

$$E/\hbar v_F = \pm \left((K_X/2 + k_x)^2 + (K_Y/2 + k_y)^2\right)^{1/2} \pm \left((K_X/2 - k_x)^2 + (K_Y/2 - k_y)^2\right)^{1/2}, \tag{3.64}$$

where $k_{x,y}$ and $K_{X,Y}$ are the wavevectors along the relative coordinates x, y and center-of mass coordinates X, Y respectively. As shown previously [245], when $K = 0$ one can move the relative motion coordinates (x, y) into polar coordinates (r, θ) such that one deals with a system of three equations only,

$$\begin{bmatrix} \frac{U(r)-E}{\hbar v_F} & \partial_r + \frac{m}{r} & 0 \\ 2\left(-\partial_r + \frac{m-1}{r}\right) & \frac{U(r)-E}{\hbar v_F} & -2\left(\partial_r + \frac{m+1}{r}\right) \\ 0 & \partial_r - \frac{m}{r} & \frac{U(r)-E}{\hbar v_F} \end{bmatrix} \begin{bmatrix} \phi_1(r) \\ \phi_2(r) \\ \phi_4(r) \end{bmatrix} = 0, \tag{3.65}$$

with $m = 0, \pm 1, \pm 2, ...$ and where one can take $\phi_3 = 0$.

Let us now consider a model potential given by $U(r) = -U_0/(1 + (r/d)^2)$, with Ohno-like on-site energy U_0, such that we can find an exact solution to the system of Eqs. (3.65). Notably this functional form is well known in optics as the spatially inhomogeneous fish-eye lens of Maxwell [261], and remarkably is the simplest exactly solvable model as the square well does not admit a nontrivial solution. When $r \sim 0$, one finds the usual short-range behavior $\phi_2 \sim r^{|m|}$, whilst the asymptotic behavior as $r \to \infty$ is given by the decay $\phi_2 \sim r^{|m|-2\eta}$, where

$$\eta = \frac{|m| + 1 + \sqrt{m^2 + 1}}{2}, \tag{3.66}$$

thus we seek a solution in the form

$$\phi_2(r) = \frac{A}{d} \times \frac{(r/d)^{|m|}}{(1 + (r/d)^2)^{\eta}} \, f(r), \tag{3.67}$$

where A is a normalization constant and $f(r)$ is some polynomial in r that does not affect the short- and long-range behavior. Upon substituting Eq. (3.67) into Eqs. (3.65), eliminating $\phi_{1,4}(r)$, and changing the variable with $\xi = (r/d)^2$ we arrive at the following equation for $f(\xi)$

$$\xi(1 + \xi)^2 f''(\xi) + (1 + \xi)\left[m + 1 + (m + 2 - 2\eta)\xi\right] f'(\xi) + \left[(\tfrac{1}{4}\tfrac{U_0 d}{\hbar v_F})^2 - \eta^2\right] f(\xi) = 0, \tag{3.68}$$

which is a form of the Gauss hypergeometric equation [79]. The solution is

$$f(\xi) = {}_2F_1\left(-n, -n + \tfrac{1}{2}\tfrac{U_0 d}{\hbar v_F}; |m| + 1; \tfrac{\xi}{1+\xi}\right), \tag{3.69}$$

where we have terminated the power series to ensure decaying solutions, leading to the following condition for bound electron-hole pairs

$$\frac{U_0 d}{\hbar v_F} = 17.2 \times d[\text{nm}] = 4(n + \eta), \quad n = 0, 1, 2... \tag{3.70}$$

where we have used the standard Ohno cut-off on-site energy [64] of 11.3 eV. Weak screening by a small number of mobile uncoupled carriers allows the system to adjust the inter-particle interaction potential so that it satisfies the strength condition given by Eq. (3.70) to support bound states, resulting in an energetically-favorable drastic reduction in the chemical potential of the many-electron system.

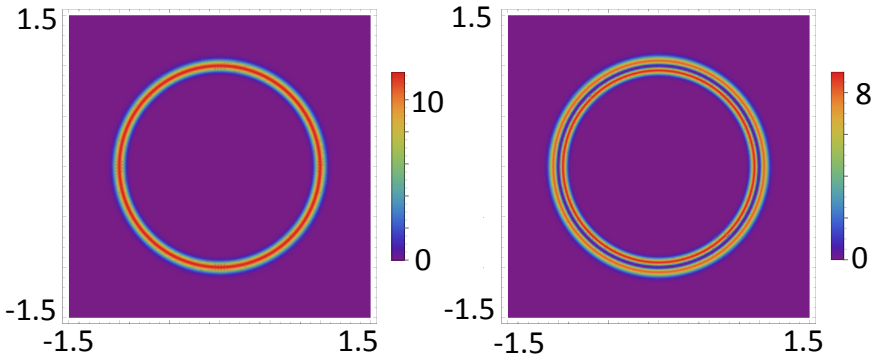

Figure 3.12: Radial probability densities for the pair states with quantum numbers $(n, m) = (0, 429), (1, 428)$ left-to-right, measured in units of d.

The other wavefunction components $\phi_{1,3,4}(r)$ are readily obtainable from Eqs. (3.65), and their long range behavior $r \to \infty$ tells us the $m = 0$ state is non-square-integrable, $(\phi_1, \phi_2, \phi_4)^T \to r^{-\sqrt{1+|m|^2}} \left(1, r^{-1}, 1\right)^T$. Thus the pair states are rotating ring-like modes.

The requirements for a monolayer exciton follow from Eq. (3.70). Due to the necessity of a metallic back gate inducing image charges, $d \approx 100$ nm, suggesting $U_0 d/\hbar v_F \approx 1718$ and so only many pair states may exist, corresponding to the quantum numbers $(n, m) = (0, 429), (1, 428), ..., (427, 2), (428, 1)$. Probability density plots are displayed in Fig. 3.12 for the two lowest node states.

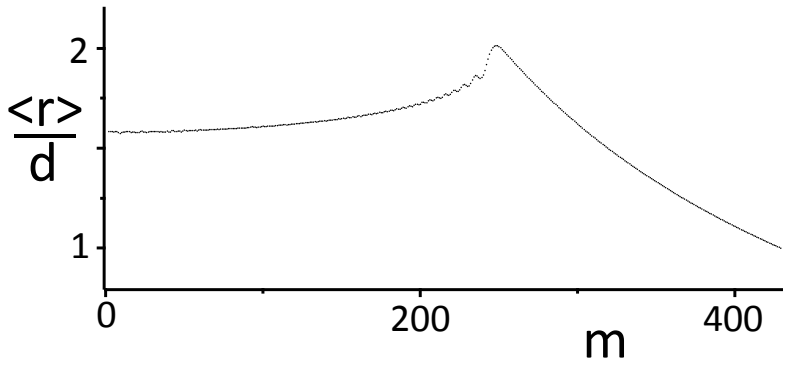

Figure 3.13: A plot of the average size of the pair state as a function of quantum number m, measure in terms of the length sale d.

The average particle separation is shown in Fig. 3.13, illustrating the minimum size of the state is d, which is found for high m states, and the maximum size is $2d$. For low m states the size of the pair is $1.6d$. Thus zero-energy bi-electronic states can exist for carrier densities n up to several units of 10^{10}cm^{-2}, whereas at higher densities they are destroyed by the Mott transition caused by overlap of the pairs. To avoid pair overlap we require $k_F d < 1$, such that we can estimate $k_F < 1/d \sim 10^7\text{m}^{-1}$ with density $n \sim k_F^2 \sim 10^{10}\text{cm}^{-2}$.

Of course, the presence of a metallic gate suggests an interaction potential with a dipole-like $(1/r^3)$ decay due to image charges. It is most convenient to deal with this situation by expanding the eigenfunctions in a Fourier-Bessel series, defined by

$$\phi_2(r) = \frac{\sqrt{2}}{L} \sum_{n=1}^{\infty} \frac{a_n}{J_{m+1}(\alpha_n)} J_m(\alpha_n \tfrac{r}{L}), \tag{3.71}$$

where α_n are roots of the Bessel function and we satisfy orthonormality over a length L, $\int_0^L \phi_2 \phi_2 r \mathrm{d}r = \delta_{n,l}$, which is taken to be large enough such that the confined state wavefunctions are insensitive to the boundary condition $\phi_2(L) = 0$. Evaluating the consequent matrix elements and solving the secular equation numerically, one finds the eigenvalues for the more realistically decaying potential $U(r) = -U_0/(1 + (r/d)^3)$ are $\frac{U_0 d}{\hbar v_F} = 7.47, 10.86, 12.70$ and so on. Another approach would be to do develop the variable phase method for two Dirac particles.

The appearance of stationary bipartite states could be of some practical importance. Indeed, a Bose-Einstein condensation of zero-energy coupled electrons or holes offers

an alternative explanation of the experimentally-seen Fermi velocity renormalization in gated graphene structures [107, 108] which is observed instead of the widely theorized gap. In this picture, the Fermi velocity renormalization is an artifact of miscalculating the number of charge carriers when the Fermi level moves towards the Dirac point energy, due to their disappearance in a mostly silent many-body ground state. A significant increase in the apparent carrier concentration in graphene in a quantizing magnetic field compared to the low-field measurements has been observed experimentally [262, 263, 264], which could be another indicator of our proposed pair states. Indeed, when the magnetic length becomes smaller than the size of a bipartite vortex, the pair breaks up and the behavior of charge carriers is defined by a strong magnetic field.

3.4.3 Conclusion

In conclusion, we have demonstrated, contrary to a widespread belief, that fully square-integrable electron-hole bound pairs are realizable at zero-energy in gapless monolayer or spatially separated two-layer graphene, despite the massless nature of the Dirac particles. These exciton states are vortices, defined by a nonzero angular momentum, and are bosonic in nature opening up the possibility for a condensate at zero-energy. The requirements on the strength and spatial extent of the interaction potential to support such excitons will likely be naturally favored to reduce the total energy of the system, perhaps via a renormalization of the Fermi velocity.

The observed puddles of charged carriers in graphene in the case of long-range disorder [110] can be treated as many-body mesoscopic domains containing condensates of bosonic bipartite vortices, thus removing the controversy of having carrier puddles despite the absence of single-particle localization due to the Klein phenomenon. Investigations of this new and unconventional many-body state, with special regard to possible occurrences of quantum critical phase transitions, will form part of a future work.

Chapter 4

Conclusions

We can only see a short distance ahead, but we can see plenty there that needs to be done.

- Alan Turing

It is a truth universally acknowledged, that a single electron in possession of a linear gapless spectrum, must be in want of a bound state. In this thesis, we have proposed several schemes to achieve a bound state in condensed matter systems with excitations described by quasi-relativistic wave equations.

The first half of this work was composed of physical situations in which one spatial dimension was most relevant. In Sec. 2.1, we treated the quasi-one dimensional Coulomb problem. We showed how the interesting phenomena of relativistic quantum mechanics, so-called atomic collapse physics, can manifest itself in 1-D Dirac materials. We hope experiments can soon be preformed to see such effects in the near future, in analogy with experiments controlling the Coulomb interaction with multiple charged impurities in graphene [93]. Sec. 2.2 laid the foundations for the area of confinement of Dirac particles via Fermi velocity engineering by detailing the solutions to a number of exactly-solvable models. With the spectacular improvements in experimental fabrication of strained mesoscopic devices [265, 266], we see no reason why such velocity barriers cannot be demonstrated in the laboratory, at least in the longer term.

The second half of this thesis encompassed studies of systems where two spatial dimensions were required to describe the prevalent physics. Confinement in inhomogeneous magnetic fields was discussed in Sec. 3.1, where it was found how both magnetic quantum dots and rings were indeed capable of trapping Dirac particles under some conditions, not previously appreciated in the literature. Forming a bound state by purely electrostatic means is widely thought to be impossible, yet in Sec. 3.2 we demonstrated how it may arise for zero-energy states, and also considered the application of a magnetic flux to the model. In Sec. 3.3, we developed a scattering theory for massless Dirac fermions based on the variable phase method and posited that optimal traps of zero-energy states are important in measurable ways, for example in resistivity. A recent experiment has reported resonant states in a photo-switchable self-assembled molecular graphene hybrid, and we believe a similar experiment could soon see truly bound states [267]. We proposed the existence of a novel and rather exotic bielectron quasiparticle in Sec. 3.4, based on an analytical solution of the quasi-relativistic quantum two-body problem. The probing of such a state has already led to preliminary discussions with a couple of leading

experimental groups [268].

4.1 Further work

There are several problems that can be tackled in the near future, either as simple extensions of the work described in this thesis, or related problems that are somewhat analogous and would compliment the areas studied here. Below we discuss both types of future work.

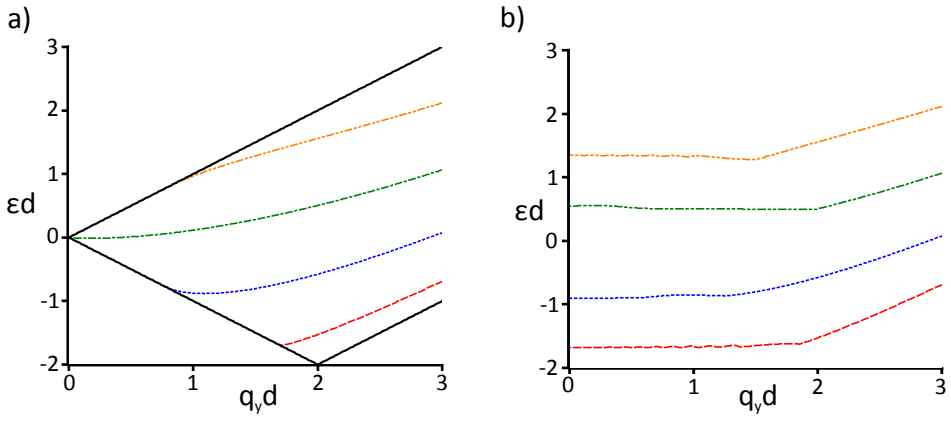

Figure 4.1: The eigenspectrum of a massless Dirac particle with transversal wavevector q_y in a 1D square well of width $2d$ and (a) vanishing magnetic field and (b) finite magnetic field. In (b) we track the states from (a) only, removing higher energy states for clarity.

In Sec. 2.1, atomic collapse was considered in a simple 1-D model. In discussions with experts in experimental carbon nanotube science, it became clear how the collapse effect changes with the application of a magnetic field is of great interest as it is a key experimental parameter than can be manipulated. Thus a treatment of an effective 1-D Coulomb interaction in a quantizing magnetic field will be the subject of future study. In fact, the associated problem of a Coulomb center in a magnetic field in 2-D materials is also in need of a fully analytic study [269]. We present in Fig. 4.1 the result of a preliminary calculation of the eigenspectrum of a Dirac-Weyl electron in a 1D potential square-well subjected a perpendicular magnetic field. One notices at high transversal wavevectors $q_d d \geq 2$ the states are highly similar to those in the nonmagnetic case, however with decreasing transversal wavevector the energy levels are bent somewhat away from purely potential well result, and quickly break out from the previously required

bound state region, defying atomic collapse.

The work of Sec. 2.1 joins a plethora of literature on one-dimensional potentials [72, 89, 90]. However as yet asymmetric potentials, which may arise in a spatially inhomogeneous dielectric environment, have been overlooked. It is known from the non-relativistic case such asymmetric potentials [270] can lead to exotic electron transport effects [271]. Therefore a detailed analytic study of asymmetric barrier is ripe for investigation. Furthermore, another phenomenon from relativistic quantum mechanics that can be expected to be realized in Dirac materials is Schwinger pair production, the particle-antiparticle creation out of the vacuum by a strong electric field [272]. Preliminary calculations have shown for a mode smooth step potential the production rate can be found analytically.

In Sec. 2.2, the work on how a spatially inhomogeneous Fermi velocity can lead to bound states can certainly be adapted to 2-D. In both cases, a more detailed study of what the strain distributions are required to realize the model velocity barriers considered is needed.

The work on unusual coupling of Dirac fermions in Sec. 3.4 can be significantly extended. The ground zero-energy state requires a full blown quantum many-body description, adapted to deal with the peculiar nature of the state. However, the quasi-relativistic two-body problem is still rich. So far, the finite energy two-body Coulomb problem has only admitted a solution for the s-state, with quantum number $m = 0$ [245]. There is a great hope for the full analytic solution with $m \neq 0$ to be found as it would lead to great insight into the full many-body problem [243], in direct analogy to Cooper pairs [273]. Remarkably, our preliminary calculations show an exact solution can be obtained in terms of confluent Heun functions [274].

The quasi-relativistic two-body problem for treating bielectrons in two dimensions necessitated the construction of a four-by-four Hamiltonian. A similar Hamiltonian written down in one dimension will allow one to describe excitons in nanostructures such as carbon nanotubes. Therefore solving the associated two-body problem and a reformulation of the Elliot formula for absorption [275] will allow one to map the absorption spectra, find the Sommerfeld factor and explain some experimental data showing peaks

that, whilst being attributed to excitons, have not yet had a solid theoretical description [276].

Finally, we briefly report on the latest interesting experimental and theoretical work. In this thesis we have completely neglected three dimensional Dirac materials. However new experiments [277, 278] have uncovered so-called 3-D Dirac semimetals, where 3-D Dirac fermions in the bulk are described by a Hamiltonian $H = v_F \left(\sigma_x p_x + \sigma_y p_y + \sigma_z p_z\right)$, opening up another dimension of exotic physics. The appearance of single valley Dirac fermions has also been demonstrated in the laboratory [279], which could be important for effects depending on the number of valleys in which Dirac fermions are present. Additionally a new type of particle, dubbed a massless Kane fermion, has been recently reported [280] in a zinc-blende crystal (HgCdTe) alongside a Hamiltonian that has no analogy in quantum electrodynamics. Perhaps more abstractly, quasiparticles following non-Abelian statistics are being increasingly studied in topological materials, examples include: Majorana fermions, parafermions, Ising anyons, Fibonacci anyons and genons [281]. Indeed, it seems for the story of new and exotic quasiparticles in condensed matter systems it is not the end, not even the beginning of the end, just perhaps the end of the beginning.

I think it's a peculiarity of myself that I like to play about with equations, just looking for beautiful mathematical relations which maybe don't have any physical meaning at all. Sometimes they do.

- Paul Dirac

Bibliography

[1] B. Thaller, *The Dirac Equation* (Springer, Berlin, 1992).

[2] P. A. M. Dirac, *Theory of Electrons and Positrons*, from *Nobel Lectures: Physics 1922-1941* (Elsevier, Amsterdam, 1965).

[3] K. S. Novoselov, Rev. Mod. Phys. **83**, 837 (2011).

[4] A. K. Geim, Rev. Mod. Phys. **83**, 851 (2011).

[5] J. Cayssol, C. R. Physique **14**, 760 (2013).

[6] T. O. Wehling, A. M. Black-Schaffer, A. V. Balatsky, Advances in Physics **63**, 1 (2014).

[7] O. Vafek and A. Vishwanath, Annu. Rev. Condens. Matter Phys. **5**, 83 (2014).

[8] M. I. Katsnelson, Eur. Phys. J. B **51**, 157 (2006).

[9] M. I. Katsnelson, K. S. Novoselov, and A. K. Geim, Nature Phys. **2**, 620 (2006).

[10] S. Q. Shen, *Topological Insulators: Dirac equation in condensed matters* (Springer-Verlag, Berlin, 2012).

[11] K. S. Novoselov, D. Jiang, F. Schedin, T. J. Booth, V. V. Khotkevich, S. V. Morozov, and A. K. Geim, Proc. Natl Acad. Sci. USA **102**, 10451 (2005).

[12] R. Saito, G. Dresselhaus, and M. S. Dresselhaus, *Physical Properties of Carbon Nanotubes* (Imperial College Press, London, 1998).

[13] Q. H. Wang, K. Kalantar-Zadeh, A. Kis, J. N. Coleman, and M. S. Strano, Nat. Nanotechnol. **7**, 699 (2012).

[14] M. Z. Hasan and C. L. Kane, Rev. Mod. Phys. **82**, 3045 (2010).

[15] X.-L. Qi and S.-C. Zhang, Rev. Mod. Phys. **83**, 1057 (2011).

[16] B. A. Volkov and O. A. Pankratov, JETP Lett. **42**, 178 (1985).

[17] F. V. Kusmartsev and A. M. Tsvelik, JETP Lett. **42**, 257 (1985).

[18] M. Konig, S. Wiedmann, C. Brune, A. Roth, H. Buhmann, L. Molenkamp, X.-L. Qi, and S.-C. Zhang, Science **318**, 766 (2007).

[19] I. Knez, R. R. Du, G. Sullivan, Phys Rev Lett **107**, 136603 (2011).

[20] W. P. Su, J. R. Schrieffer and A. Heeger, Phys. Rev. Lett. **42**, 1698 (1979).

[21] G. E. Volovik, *Exotic properties of superfluid 3He* (World Scientific, Singapore, 1992).

[22] A. V. Balatsky, I. Vekhter, and J. X. Zhu, Rev. Mod. Phys. **78**, 373 (2006).

[23] L. Tarruell, D. Greif, T. Uehlinger, G. Jotzu and T. Esslinger, Nature **483**, 302 (2012).

[24] M. Bellec, U. Kuhl, G. Montambaux and F. Mortessagne, Phys. Rev. Lett. **110**, 033902 (2013).

[25] O. Peleg, G. Bartal, B. Freedman, O. Manela, M. Segev and D. N. Christodoulides, Phys. Rev. Lett. **98**, 103901 (2007).

[26] G. Weick, C. Woollacott, W. L. Barnes, O. Hess, and E. Mariani, Phys. Rev. Lett. **110**, 106801 (2013).

[27] T. J. Sturges, C. Woollacott, G. Weick, and E. Mariani, 2D Mater. **2**, 014008 (2015).

[28] K. K. Gomes, W. Mar, W. Ko, F. Guinea and H. C. Manoharan, Nature **483**, 306 (2012).

[29] M. Gibertini, A. Singha, V. Pellegrini, M. Polini, G. Vignale, A. Pinczuk, L. N. Pfeiffer and K. W. West, Phys. Rev. B **79**, 241406(R) (2009).

[30] T. Ando and T. Nakanishi, J. Phys. Soc. Jpn. **67**, 1704 (1998); T. Ando, T. Nakanishi, and R. Saito, *ibid.* **67**, 2857 (1998).

[31] O. Klein, Z. Phys. **53**, 157 (1929).

[32] A. Calogeracos and N. Dombey, Contemp. Phys. **40**, 313 (1999).

[33] A. Calogeracos and N. Dombey, Int. J. Mod. Phys. A **14**, 631 (1999).

[34] N. Dombey and A. Calogeracos, Phys. Rep. **315**, 41 (1999).

[35] D. Dragoman, Phys. Scr. **79**, 015003 (2009).

[36] N. Bohr, Phil. Mag. **26**, 1 (1913).

[37] E. Schrödinger, Ann. Phys. (Berlin) **79**, 361 (1926); *ibid*. **79**, 489 (1926).

[38] W. Pauli, Z. Phys. **36**, 336 (1926).

[39] L. D. Landau and E. M. Lifshitz, *Quantum Mechanics* (Pergamon Press, New York, 1977).

[40] S. Flügge and H. Marschall, *Rechenmethoden der Quantentheorie* (Springer Verlag, Berlin, 1952).

[41] X. L. Yang, S. H. Guo, F. T. Chan, K. W. Wong, and W. Y. Ching, Phys. Rev. A **43**, 1186 (1991).

[42] D. G. W. Parfitt and M. E. Portnoi, J. Math. Phys. **43**, 4681 (2002).

[43] A. J. Makowski, Phys. Rev. A **84**, 022108 (2011).

[44] R. Loudon, Am. J. Phys. **27**, 649 (1959).

[45] M. Andrews, Am. J. Phys. **34**, 1194 (1966).

[46] L. K. Haines and D. H. Roberts, Am. J. Phys. **37**, 1145 (1969).

[47] P. A. M. Dirac, Proc. R. Soc. London, Ser. A **117**, 610 (1928); *ibid*. **118**, 351 (1928).

[48] W. Gordon, Z. Phys. **48**, 11 (1928); C. G. Darwin, Proc. R. Soc. London A **118**, 654 (1928).

[49] L. D. Landau and E. M. Lifshitz, *Quantum Electrodynamics* (Pergamon Press, Oxford, 1975).

[50] S. H. Guo, X. L. Yang, F. T. Chan, K. W. Wong, and W. Y. Ching, Phys. Rev. A **43**, 1197 (1991).

[51] S. H. Dong and Z. Q. Ma, Phys. Lett. A **312**, 78 (2003).

[52] V. P. Krainov, Sov. Phys. JETP **37**, 406 (1973).

[53] H. N. Spector and J. Lee, Am. J. Phys. **53**, 248 (1985).

[54] D. S. Miserev and M. V. Entin, JETP **115**, 694 (2012).

[55] A. V. Shytov, M. I. Katsnelson, and L. S. Levitov, Phys. Rev. Lett. **99**, 236801 (2007)

[56] A. V. Shytov, M. I. Katsnelson, and L. S. Levitov, Phys. Rev. Lett. **99**, 246802 (2007).

[57] A. H. Castro Neto, F. Guinea, N. M. R. Peres, K. S. Nososelov, and A. K. Geim, Rev. Mod. Phys. **81**, 109 (2009).

[58] M. I. Katsnelson, Phys. Rev. B **74**, 201401 (2006).

[59] D. Xiao, G.-B. Liu, W. Feng, X. Xu, and W. Yao, Phys. Rev. Lett. **108**, 196802 (2012).

[60] J. C. Charlier, X. Blase, and S. Roche, Rev. Mod. Phys. **79**, 677 (2007).

[61] S. M. Young, S. Zaheer, J. C. Y. Teo, C. L. Kane, E. J. Mele, and A. M. Rappe, Phys. Rev. Lett. **108**, 140405 (2012).

[62] K. C. Yung, W. M. Wu, M. P. Pierpoint and F. V . Kusmartsev, Contemp. Phys. **54**, 233 (2013).

[63] L. Bányai, I. Galbraith, C. Ell, and H. Haug, Phys. Rev. B **36**, 6099 (1987).

[64] V. Perebeinos, J. Tersoff, and P. Avouris, Phys. Rev. Lett. **92**, 257402 (2004),

[65] A. V. Turbiner, Commun. Math. Phys. **118**, 467 (1988).

[66] C. A. Downing, J. Math. Phys. **54**, 072101 (2013).

[67] F. Domínguez-Adame and A. Rodríguez, Phys. Lett. A **198**, 275 (1995).

[68] R. R. Hartmann, N. J. Robinson, and M. E. Portnoi, Phys. Rev. B **81**, 245431 (2010).

[69] R. R. Hartmann, I. A. Shelykh, and M. E. Portnoi Phys. Rev. B **84**, 035437 (2011).

[70] H. Haug and S. W. Koch, *Quantum Theory of the Optical and Electronic Properties of Semiconductors* (World Scientific, Singapore, 2004).

[71] M. Barbier, F. M. Peeters, P. Vasilopoulos, and J. M. Pereira Jr., Phys. Rev. B **77**, 115446 (2008).

[72] V. V. Cheianov and V. I. Falko, Phys. Rev. B **74**, 041403(R) (2006).

[73] K. J. A. Reijnders, T. Tudorovskiy, and M. I. Katsnelson, Ann. Phys. **333**, 155 (2013).

[74] Y. Zhong and G. L. Gao, J. Math. Phys. **54**, 043510 (2013).

[75] M. E. Portnoi, C. A. Downing, R. R. Hartmann and I. A. Shelykh, Int. Conf. on Electromagnetics in Advanced Applications (ICEAA) pp 2314, (2013).

[76] R. J. Downes, M. Levitin, and D. Vassiliev, J. Math. Phys. **54**, 111503 (2013).

[77] K. Pankrashkin, S. Richard, J. Math. Phys. **55**, 062305 (2014).

[78] V. Jakubský and D. Krejcirk, Annals of Physics **349**, 268 (2014).

[79] I. S. Gradshteyn and I. M. Ryzhik, *Table of Integrals, Series and Products* (Academic, New York, 1980).

[80] L. I. Schiff, H. Snyder, and J. Weinberg, Phys. Rev. **57**, 315 (1940).

[81] I. Pomeranchuk and Y. Smorodinsky, J. Phys. **9**, 97 (1945).

[82] Y. B. Zeldovich and V. S. Popov, Sov. Phys. Usp. **14**, 673 (1972).

[83] Y. Li, S. V. Rotkin, and U. Ravaioli, Nano Lett. **3**, 183 (2003).

[84] D. Gunlycke, C. J. Lambert, S. W. D. Bailey, D. G. Pettifor, G. A. D. Briggs, and J. H. Jefferson, Europhys. Lett. **73**, 759 (2006).

[85] H. Ajiki and T. Ando, Physica B **201**, 349 (1994).

[86] G. Fedorov, A. Tselev, D. Jimenez, S. Latil, N. G. Kalugin, P. Barbara, D. Smirnov, and S. Roche, Nano Lett. **7**, 960 (2007).

[87] M. E. Portnoi, O. V. Kibis, M. Rosenau da Costa, Superlattices and Microstructures **43**, 399 (2008).

[88] M. E. Portnoi, M. Rosenau da Costa, O. V. Kibis, and I. A. Shelykh, Int. Journ. Mod. Phys. B **23**, 2846 (2009).

[89] J. M. Pereira Jr., V. Mlinar, F. M. Peeters, and P. Vasilopoulos, Phys. Rev. B **74**, 045424 (2006).

[90] T. Ya. Tudorovskiy and A. V. Chaplik, JETP Lett. **84**, 619 (2006).

[91] L.-J. Li, R. J. Nicholas, R. S. Deacon, and P. A. Shields, Phys. Rev. Lett. **93**, 156104 (2004).

[92] L. Brey and H. A. Fertig, Phys. Rev. B **73**, 235411 (2006).

[93] Y. Wang, D. Wong, A. V. Shytov, V. W. Brar, C. Sangkook, Q. Wu, H. Z. Tsai, W. Regan, A. Zettl, R. K. Kawakami, S. G. Louie, L. S. Levitov, and M. F. Crommie, Science **340**, 734 (2013).

[94] O. I. Siidra, D. O. Zinyakhina, A. I. Zadoya , S. V. Krivovichev, and R. W. Turner, Inorg. Chem. **52**, 12799 (2013).

[95] F. de Juan, A. Cortijo, and M. A. H. Vozmediano, Phys. Rev. B **76**, 165409 (2007).

[96] N. M. R. Peres, J. Phys.: Condens. Matter **21**, 095501 (2009).

[97] A. Concha and Z. Tešanović, Phys. Rev. B **82**, 033413 (2010).

[98] A. Raoux, M. Polini, R. Asgari, A. R. Hamilton, R. Fazio, and A. H. MacDonald, Phys. Rev. B **81**, 073407 (2010).

[99] P. M. Krstajić and P. Vasilopoulos, J. Phys.: Condens. Matter **23**, 135302 (2011).

[100] F. M. D. Pellegrino, G. G. N. Angilella, and R. Pucci, Phys. Rev. B **84**, 195404 (2011).

[101] L. Liu, Y.-X. Li, J.-J. Liu, Physics Letters A **376**, 3342 (2012).

[102] J.-H. Yuan, J.-J. Zhang, Q.-J. Zeng, J.-P. Zhang, Z. Cheng, Physica B **406**, 4214 (2011).

[103] J. R. F. Lima, F. Moraes, Solid State Commun. **201**, 82 (2015).

[104] J. H. Yuan, Z. Cheng, Q. J. Zeng, J. P. Zhang, and J. J. Zhang, J. Appl. Phys. **110**, 103706 (2011).

[105] Y. Wang, Y. Liu, B. Wang, Physica E **48**, 191 (2013).

[106] H. Cheraghchi and F. Adinehvand, J. Phys.: Condens. Matter **26**, 015302 (2014).

[107] D. C. Elias, R. V. Gorbachev, A. S. Mayorov, S. V. Morozov, A. A. Zhukov, P. Blake, L. A. Ponomarenko, I. V. Grigorieva, K. S. Novoselov, F. Guinea, and A. K. Geim, Nature Phys. **7**, 701 (2011).

[108] D. A. Siegel, C. Park, C. Hwang, J. Deslippe, A. V. Fedorov, S. G. Louie, and A. Lanzara, Proc. Natl. Acad. Sci. U.S.A. **108**, 11365 (2011).

[109] F. de Juan, M. Sturla, and M. A. H. Vozmediano, Phys. Rev. Lett. **108**, 227205 (2012).

[110] J. Martin, N. Akerman, G. Ulbricht, T. Lohmann, J. H. Smet, K. von Klitzing, and A. Yacoby, Nat. Phys. **4**, 144 (2008).

[111] A. Luican, G. Li, and E. Y. Andrei, Phys. Rev. B **83**, 041405(R) (2011).

[112] C.-H. Park, L. Yang, Y.-W. Son, M. L. Cohen, and S. G. Louie, Nat. Phys. **4**, 213 (2008).

[113] H. Yan, Z.-D. Chu, W. Yan, M. Liu, L. Meng, M. Yang, Y. Fan, J. Wang, R.-F. Dou, Y. Zhang, Z. Liu, J.-C. Nie, and L. He, Phys. Rev. B **87**, 075405 (2013).

[114] L. Tapasztó, G. Dobrik, P. Nemes-Incze, G. Vertesy, Ph. Lambin, and L. P. Biró, Phys. Rev. B **7**, 233407 (2008).

[115] W.-J. Jang, H. Kim, Y.-R. Shin, M. Wang, S. K. Jang, M. Kim, S. Lee, S.-W. Kim, Y. J. Song, S.-J. Kahng, Carbon **74** 139, (2014).

[116] L. Liu, Y.-X. Li, Y.-T. Zhang, and J.-J. Liu, Journal of Applied Physics, **115**, 023704 (2014).

[117] W. Gerlach and O. Stern, Zeitschrift für Physik **9**, 353 (1922).

[118] A. D. Sakharov and I. E. Tamm, Fizika plazmy i problema upravlyaemykh termoyadernykh reaktsi (Plasma Physics and the Control of Thermonuclear Reactions), 1, AN SSSR, 3 (1951).

[119] M. V. Berry and A. K. Geim, Eur. J. Phys **18**, 307 (1997).

[120] J. W. McClure, Phys. Rev. **104**, 666 (1956).

[121] F. D. M. Haldane, Phys. Rev. Lett. **61**, 2015 (1988).

[122] Y. Zheng and T. Ando, Phys. Rev. B **65**, 245420 (2002).

[123] H.-Y. Chen, V. Apalkov, and T. Chakraborty, Phys. Rev. Lett. **98**, 186803 (2007).

[124] K. S. Novoselov, A. K. Geim, S. V. Morozov, D. Jian, M. I. Katsnelson, I. V. Grigorieva, S. V. Dubonos, and A. A. Firsov, Nature **438**, 197 (2005).

[125] K. I. Bolotin, F. Ghahari, M. D. Shulman, H. L. Stormer, and P. Kim, Nature **462**, 196 (2009).

[126] A. F. Young, J. D. Sanchez-Yamagishi, B. Hunt, S. H. Choi, K. Watanabe, T. Taniguchi, R. C. Ashoori, P. Jarillo-Herrero, Nature **505**, 528 (2014).

[127] A. V. Rozhkov, G. Giavaras,Y. P. Bliokh,V. Freilikher, and F. Nori, Phys. Rep. **503**, 77 (2011).

[128] S. J. Lee, S. Souma, G. Ihm, and K. J. Chang, Phys. Rep. **394**, 1 (2004).

[129] A. Nogaret, J. Phys. Condens. Matter **22**, 253201 (2010).

[130] L. Oroszlany, P. Rakyta, A. Kormanyos, C. J. Lambert, and J. Cserti, Phys. Rev. B **77**, 081403(R) (2008).

[131] T. K. Ghosh, A. De Martino, W. Hausler, L. DellAnna, and R. Egger, Phys. Rev. B **77**, 081404(R) (2008).

[132] S. Park and H.-S. Sim, Phys. Rev. B **77**, 075433 (2008).

[133] A. Kormanyos, P. Rakyta, L. Oroszlany, and J. Cserti, Phys. Rev. B **78**, 045430 (2008).

[134] S. Ghosh and M. Sharma, J. Phys.: Condens. Matter **21**, 292204 (2009).

[135] S. Kuru, J. Negro and L. M. Nieto, J. Phys.: Condens. Matter **21**, 455305 (2009).

[136] T. K. Ghosh, J. Phys.: Condens. Matter **21** 045505 (2009).

[137] E. Milpas, M. Torres and G. Murguia, J. Phys.: Condens. Matter **23**, 245304 (2011).

[138] D. Wang and G. Jin, EPL **88**, 17011 (2009).

[139] A. De Martino, L. DellAnna, and R. Egger, Phys. Rev. Lett. **98**, 066802 (2007).

[140] D. Wang and G. Jin, Phys Lett. A **373**, 4082 (2009).

[141] C. M. Lee, R. C. H. Lee, W. Y. Ruan, and M. Y. Chou, Appl. Phys. Lett. **96**, 212101 (2010).

[142] M. Ramezani Masir, A. Matulis, and F. M. Peeters, Phys. Rev. B **79**, 155451 (2009).

[143] A. M. Essin and D. J. Griffiths, Am. J. Phys. **74**, 109 (2006).

[144] C. A. Downing, Cent. Eur. J. Phys. **11**, 977 (2013).

[145] P. D. Ye, D. Weiss, R. R. Gerhardts, M. Seeger, K. von Klitzing, K. Eberl, and H. Nickel, Phys. Rev. Lett. **74**, 3013 (1995).

[146] H. A. Carmona, A. K. Geim, A. Nogaret, P. C. Main, T. J. Foster, M. Henini, S. P. Beaumont, and M. G. Blamire, Phys. Rev. Lett. **74**, 3009 (1995).

[147] C. L. Foden, M. L. Leadbeater, J. H. Burroughes and M. Pepper J. Phys.: Condens. Matter **6**, L127 (1994).

[148] P. Roy, T. K. Ghosh and K. Bhattacharya, J. Phys. Condens. Matter **24**, 055301 (2012).

[149] A. Ronveaux, *Heun's Differential Equations* (Oxford University Press, Oxford, 1995).

[150] A. F. Young and P. Kim, Nat. Phys. **5**, 222 (2009).

[151] T. Tudorovskiy, K. J. A. Reijnders, and M. I. Katsnelson, Phys. Scr. T **146**, 014010 (2012).

[152] M. Ramezani Masir, P. Vasilopoulos, A. Matulis, and F. M. Peeters, Phys. Rev. B. **77**, 235443 (2008).

[153] P. Recher, J. Nilsson, G. Burkard, and B. Trauzettel, Phys. Rev. B **79**, 085407 (2009).

[154] P. Recher, B. Trauzettel, A. Rycerz, Y. M. Blanter, C. W. J. Beenakker, and A. F. Morpurgo, Phys. Rev. B **76**, 235404 (2007).

[155] J. Schelter, D. Bohr, and B. Trauzettel, Phys. Rev. B **81**, 195441 (2010).

[156] J. Wurm, M. Wimmer, H. U. Baranger, and K. Richter, Semicond. Sci. Technol. **25**, 034003 (2010).

[157] J. Schelter, P. Recher, B. Trauzettel, Solid State Commun. **152**, 1411 (2012).

[158] S. Russo, J. B. Oostinga, D. Wehenkel, H. B. Heersche, S. S. Sobhani, L. M. K. Vandersypen, and A. F. Morpurgo, Phys. Rev. B. **77**, 085413 (2008).

[159] M. Huefner, F. Molitor, A. Jacobsen, A. Pioda, C. Stampfer, K. Ensslin, and T. Ihn, New J. Phys. **12**, 043054 (2010).

[160] J. H. Bardarson, M. Titov, and P. W. Brouwer, Phys. Rev. Lett. **102**, 226803 (2009).

[161] A. Cresti, F. Ortmann, T. Louvet, D. Van Tuan, and S. Roche, Phys. Rev. Lett. **110**, 196601 (2013).

[162] C. Y. Hou, C. Chamon, and C. Mudry, Phys. Rev. Lett. **98**, 186809 (2007).

[163] R. Jackiw, Phys. Scr. **T146**, 014005 (2012).

[164] V. M. Pereira, J. Nilsson, and A. H. Castro Neto, Phys. Rev. Lett. **99**, 166802 (2007).

[165] K. S. Gupta and S. Sen, Phys. Rev. B **78**, 205429 (2008).

[166] K. S. Gupta, A. Samsarov, and S. Sen, Eur. Phys. J. B **73**, 389 (2010).

[167] K. S. Gupta, E. Harikumar and A. R. de Queiroz, EPL **102**, 10006 (2013).

[168] B. Chakraborty, K. S. Gupta, and S. Sen, Phys. Rev. B **83**, 115412 (2011).

[169] J. Heinl, M. Schneider, and P. W. Brouwer , Phys. Rev. B. **87**, 245426 (2013).

[170] J. G. Russo and A. A. Tseytlin, Nucl. Phys. **B461**, 131 (1996).

[171] D. Garfinkle, S. B. Giddings, and A. Strominger, Phys. Rev. D **49**, 958 (1994).

[172] S. J. Bending, K. von Klitzing, and K. Ploog, Phys. Rev. Lett. **65**, 1060 (1990).

[173] J. Grundberg, T. H. Hansson, A. Karlhede and J. M. Leinaas, Mod. Phys. Lett. B **5**, 539 (1991).

[174] V. M. Fomin, *Physics of Quantum Rings* (Springer, Heidelberg, 2014).

[175] A. M. Fischer, V. L. Campo, Jr., M. E. Portnoi, and R. A. Roemer, Phys. Rev. Lett. **102**, 096405 (2009).

[176] A. M. Aleexev and M. E. Portnoi, Phys. Rev. B **85**, 245419 (2012).

[177] A. M. Aleexev, I. A. Shelykh and M. E. Portnoi, Phys. Rev. B **88**, 085429 (2013).

[178] A. Fert, Rev. Mod. Phys. **80**, 1517 (2008).

[179] P. A. Grunberg, Rev. Mod. Phys. **80**, 1531 (2008).

[180] K. S. Novoselov, A. K. Geim, S. V. Morozov, D. Jiang, Y. Zhang, S. V. Dubonos, I. V. Gregorieva, and A. A. Firsov, Science **306**, 666 (2004).

[181] D. S. L. Abergel, V. Apalkov, J. Berashevich, K. Ziegler, and T. Chakraborty, Adv. Phys. **59**, 261 (2010).

[182] P. Hewageegana and V. Apalkov, Phys. Rev. B **77**, 245426 (2008).

[183] C. A. Downing and M. E. Portnoi, Phys. Rev. A **90**, 052116 (2014).

[184] S. Adam, E. H. Hwang, E. Rossi, and S. Das Sarma, Solid State Commun. **149**, 1072 (2009).

[185] N. M. R. Peres, Rev. Mod. Phys. **82**, 2673 (2010).

[186] S. Das Sarma, S. Adam, E. H. Hwang, and E. Rossi, Rev. Mod. Phys. **83**, 407 (2011).

[187] F. Withers, M. Dubois, and A. K. Savchenko, Phys. Rev. B **82**, 073403 (2010).

[188] Z. H. Ni, T. Yu, Y. H. Lu, Y. Y. Wang, Y. P. Feng, and Z. X. Shen, ACS Nano **2**, 2301 (2008).

[189] Y. Wang, V. W. Brar, A. V. Shytov, Q. Wu, W. Regan, H. Z. Tsai, A. Zettl, L. S. Levitov and M. F. Crommie, Nat. Phys. **8**, 653 (2012).

[190] M. I. Katsnelson and K. S. Novoselov, Solid State Commun. **143**, 3 (2007).

[191] M. I. Katsnelson and A. K. Geim, Philos. Trans. R. Soc. London, Ser. A **366**, 195 (2008).

[192] D. S. Novikov, Phys. Rev. B **76**, 245435 (2007).

[193] F. Guinea, J. Low Temp. Phys. **153**, 359 (2008).

[194] D. M. Basko, Phys. Rev. B **78**, 115432 (2008).

[195] M. Titov, P. M. Ostrovsky, I. V. Gornyi, A. Schuessler, and A. D. Mirlin, Phys. Rev. Lett. **104**, 076802 (2010).

[196] P. M. Ostrovsky, M. Titov, S. Bera, I. V. Gornyi, and A. D. Mirlin, Phys. Rev. Lett. **105**, 266803 (2010).

[197] T. O. Wehling, S. Yuan, A. I. Lichtenstein, A. K. Geim, and M. I. Katsnelson, Phys. Rev. Lett. **105**, 056802 (2010).

[198] M. Schneider and P. W. Brouwer, Phys. Rev. B **84**, 115440 (2011).

[199] L. A. Ponomarenko, R. Yang, T. M. Mohiuddin, M. I. Katsnelson, K. S. Novoselov, S. V. Morozov, A. A. Zhukov, F. Schedin, E. W. Hill, and A. K. Geim, Phys. Rev. Lett. **102**, 206603 (2009).

[200] J. H. Chen, W. G. Cullen, C. Jang, M. S. Fuhrer, and E. D. Williams, Phys. Rev. Lett. **102**, 236805 (2009).

[201] Z. H. Ni, L. A. Ponomarenko, R. R. Nair, R. Yang, S. Anissimova, I. V. Grigorieva, F. Schedin, Z. X. Shen, E. H. Hill, K. S. Novoselov, and A. K. Geim, Nano Lett. **10**, 3868 (2010).

[202] M. Monteverde, C. Ojeda-Aristizabal, R. Weil, K. Bennaceur, M. Ferrier, S. Guéron, C. Glattli, H. Bouchiat, J. N. Fuchs, and D. L. Maslov, Phys. Rev. Lett. **104**, 126801 (2010).

[203] V. V. Zalipaev, D. N. Maksimov, C. M. Linton, F. V. Kusmartsev, Phys. Lett. A **377**, 216 (2013).

[204] A. Deshpande and B. J. Le Roy, Physica E **44**, 743-759 (2012).

[205] M. M. Fogler, D. S. Novikov, and B. I. Shklovskii, Phys. Rev. B **76**, 233402 (2007).

[206] F. Calogero, *Variable Phase Approach to Potential Scattering* (Academic, New York, 1967).

[207] V. Babikov, *Method of the Phase Functions in Quantum Mechanics* (Nauka, Moscow, 1971).

[208] M. E. Portnoi, Pisma Zh. Tekh. Fiz. **14**, 1252 (1988); [Sov. Tech. Phys. Lett. **14**, 547 (1988)].

[209] M. E. Portnoi and I. Galbraith, Solid State Commun. **103**, 325 (1997).

[210] M. E. Portnoi and I. Galbraith, Phys. Rev. B **60**, 5570 (1999).

[211] H. Ouerdane, R. Varache, M. E. Portnoi and I. Galbraith, Eur. Phys. J. B **65**, 195 (2008).

[212] P. M. Morse and W. P. Allis, Phys. Rev. **44**, 269 (1933).

[213] D. A. Stone, C. A. Downing, and M. E. Portnoi, Phys. Rev. B **86**, 075464 (2012).

[214] N. Levinson, K. Dans. Vidensk. Selsk. Mat. Fys. Medd. **25**, 3 (1949).

[215] R. G. Newton, *Scattering Theory of Waves and Particles*, (Dover Publications, New York, 2002).

[216] J. Friedel, Philos. Mag. **43**, 153 (1952).

[217] F. G. Fumi, Philos. Mag. **46**, 1007 (1955).

[218] A. Zazunov, A. Kundu, A. Hütten, and R. Egger, Phys. Rev. B **82**, 155431 (2010).

[219] M. Ramezani Masir, P. Vasilopoulos, and F. M. Peeters, J. Phys. Condens. Matter **23**, 315301 (2011).

[220] M. Abramowitz and I. Stegun, *Handbook of Mathematical Functions* (Dover, New York, 1972).

[221] S. Y. Zhou, G. H. Gweon, A. V. Fedorov, P. N. First, W. A. de Heer, D. H. Lee, F. Guinea, A. H. Castro Neto, and A. Lanzara, Nat. Mater. **6**, 770 (2007).

[222] C. W. J. Beenakker, Annu. Rev. Con. Mat. Phys. **4**, 113 (2013).

[223] Q. Lin, Phys. Rev. A. **57**, 3478 (1998).

[224] S. Dong, X. Hou and Z. Ma , Phys. Rev. A **58**, 2160 (1998).

[225] C. A. Downing, D. A. Stone, and M. E. Portnoi, Phys. Rev. B **84**, 155437 (2011).

[226] M. Zarenia, A. Chaves, G. A. Farias, and F. M. Peeters, Phys. Rev. B **84**, 245403 (2011).

[227] M. Grujić, M. Zarenia, A. Chaves, M. Tadić, G. A. Farias, and F. M. Peeters, Phys. Rev. B **84**, 205441 (2011).

[228] G. Parzen, Phys. Rev. **80**, 261 (1950).

[229] L. A. Ponomarenko, A. K. Geim, A. A. Zhukov, R. Jalil, S. V. Morozov, K. S. Novoselov, I. V. Grigorieva, E. H. Hill, V. V. Cheianov, V. I. Falko, K. Watanabe, T. Taniguchi, and R. V. Gorbachev, Nat. Phys. **7**, 958 (2011).

[230] L. Britnell, R. V. Gorbachev, R. Jalil, B. D. Belle, F. Schedin, A. Mishchenko, T. Georgiou, M. I. Katsnelson, L. Eaves, S. V. Morozov, N. M. R. Peres, J. Leist, A. K. Geim, K. S. Novoselov, and L. A. Ponomarenko, Science **335**, 947 (2012).

[231] R. V. Gorbachev, A. K. Geim, M. I. Katsnelson, K. S. Novoselov, T. Tudorovskiy, I. V. Grigorieva, A. H. MacDonald, K. Watanabe, T. Taniguchi, and L. A. Ponomarenko, Nat. Phys. **8**, 896 (2012).

[232] M. Titov, R. V. Gorbachev, B. N. Narozhny, T. Tudorovskiy, M. Schtt, P. M. Ostrovsky, I. V. Gornyi, A. D. Mirlin, M. I. Katsnelson, K. S. Novoselov, A. K. Geim, and L. A. Ponomarenko, Phys. Rev. Lett. **111**, 166601 (2013).

[233] B. N. Narozhny, M. Titov, I. V. Gornyi, and P. M. Ostrovsky, Phys. Rev. B **85**, 195421 (2012).

[234] J. C. W. Song and L. S. Levitov, Phys. Rev. Lett. **109**, 236602 (2012).

[235] J. C. W. Song and L. S. Levitov, Phys. Rev. Lett. **111**, 126601 (2013).

[236] J. C. W. Song, D. A. Abanin, and L. S. Levitov, Nano Lett. **13**, 3631 (2013).

[237] M. Schutt, P. M. Ostrovsky, M. Titov, I. V. Gornyi, B. N. Narozhny, and A. D. Mirlin, Phys. Rev. Lett. **110**, 026601 (2013).

[238] D. V. Khveshchenko, Phys. Rev. Lett. **87**, 246802 (2001).

[239] J. Gonzalez, F. Guinea, and M. A. H. Vozmediano, Nucl. Phys. **424**, 595 (1994).

[240] J. Gonzalez, F. Guinea, and M. A. H. Vozmediano, Phys. Rev. B **59**, 2474(R) (1999).

[241] E. V. Gorbar, V. P. Gusynin, V. A. Miransky, and I. A. Shovkovy, Phys. Rev. B **66**, 045108 (2002).

[242] J. E. Drut, and T. A. Lahde, Phys. Rev. Lett. **102**, 026802 (2009).

[243] V. N. Kotov, B. Uchoa, V. M. Pereira, A. H. Castro Neto, F. Guinea, Rev. Mod. Phys. **84**, 1067 (2012).

[244] J. Wang, H. A. Fertig, G. Murthy, and L. Brey, Phys. Rev. B. **83**, 035404 (2011).

[245] J. Sabio, F. Sols, and F. Guinea, Phys. Rev. B **82**, 121413(R) (2010).

[246] R. N. Lee, A. I. Milstein, and I. S. Terekhov, Phys. Rev. B **86**, 035425 (2012).

[247] P. V. Ratnikov and A. P. Silin, JETP **114**, 512 (2012).

[248] M. M. Mahmoodian and M. V. Entin, Nanoscale Research Letters **7**, 599 (2012).

[249] M. M. Mahmoodian and M. V. Entin, EPL **102**, 37012 (2013).

[250] A. S. Mayorov, D. C. Elias, I. S. Mukhin, S. V. Morozov, L. A. Ponomarenko, K. S. Novoselov, A. K. Geim, R. V. Gorbachev, Nano Lett. **12**, 4629 (2012).

[251] O. L. Berman, Y. E. Lozovik, and G. Gumbs, Phys. Rev. B **77**, 155433 (2008).

[252] O. L. Berman, R. Y. Kezerashvili, and K. Ziegler, Phys. Rev. B **85**, 035418 (2012).

[253] O. L. Berman, R. Y. Kezerashvili, and K. Ziegler, Phys. Rev. B **86**, 235404 (2012).

[254] O. L. Berman, R. Y. Kezerashvili, and K. Ziegler, Phys. Rev. A **87**, 042513 (2013).

[255] Yu. E. Lozovik, S. L. Ogarkov, and A. A. Sokolik, Phil. Trans. R. Soc. A **368**, 5417 (2010).

[256] D. K. Efimkin and Yu. E. Lozovik, J. Exp. Theoret. Phys. **113**, 880 (2011).

[257] Yu. E. Lozovik, S. L. Ogarkov, and A. A. Sokolik, Phys. Rev. B **86**, 045429 (2012).

[258] C. A. Downing, A. R. Pearce, R. J. Churchill and M. E. Portnoi, arXiv:1503.08200 (2015).

[259] R. Asgari, M. I. Katsnelson, and M. Polini, Ann. Phys. (Berlin) **526**, 359 (2014).

[260] J. H. Grönqvist, T. Stroucken, G. Berghuser, S. W. Koch, arXiv:1107.5653 (2011).

[261] J. C. Maxwell, Cambridge Dublin Math. J. **8**, 188 (1854).

[262] T. J. B. M. Janssen, A. Tzalenchuk, R. Yakimova, S. Kubatkin, S. Lara-Avila, S. Kopylov, and V. I. Falko, Phys. Rev. B **83**, 233402 (2011).

[263] N. V. Agrinskaya, V. A. Berezovets, V. I. Kozub, I. S. Kotousova, A. A. Lebedev, S. P. Lebedev, A. A. Sitnikova, Semiconductors **47**, 301 (2013).

[264] J. A. Alexander-Webber, A. M. R. Baker, T. J. B. M. Janssen, A. Tzalenchuk, S. Lara-Avila, S. Kubatkin, R. Yakimova, B. A. Piot, D. K. Maude, and R. J. Nicholas, Phys. Rev. Lett. **111**, 096601 (2013).

[265] H. H. P. Garza, E. W. Kievit, G. F. Schneider, and U. Staufer, Nano Lett. **14**, 4107 (2014).

[266] H. Shioya, M. F. Craciun, S. Russo, M. Yamamoto, and S. Tarucha, Nano Lett. **14**, 1158 (2014).

[267] E. Margapoti, P. Strobel, M. M. Asmar, M. Seifert, J. Li, M. Sachsenhauser, O. Ceylan, C.-A. Palma, J. V. Barth, J. A. Garrido, A. Cattani-Scholz, S. E. Ulloa, and J. J. Finley, Nano Lett. **14**, 6823 (2014).

[268] R. J. Nicholas and L. A. Ponomarenko (private communications).

[269] O. V. Gamayun, E. V. Gorbar and V. P. Gusynin, Phys. Rev. B **83**, 235104 (2011).

[270] O. V. Kibis, Pisma Zh. ksp. Teor. Fiz. **66**, 551 (1997); [JETP Lett. **66**, 588 (1997)].

[271] A. G. Pogosov, M. V. Budantsev, O. V. Kibis, A. Pouydebasque, D. K. Maude, and J. C. Portal, Phys. Rev. B **61**, 15603 (2000).

[272] J. Schwinger, Phys. Rev. **82**, 664 (1951).

[273] L. N. Cooper, Phys. Rev. **104**, 1189 (1956).

[274] C. A. Downing and M. E. Portnoi (unpublished).

[275] R. J. Elliott, Phys. Rev. **108**, 1384 (1957).

[276] E. H. Haroz, J. G. Duque, X. Tu, M. Zheng, A. R. Hight Walker, R. H. Hauge, S. K. Doorn, J. Kono, Nanoscale **5**, 1411 (2013).

[277] Z. K. Liu, B. Zhou, Y. Zhang, Z. J. Wang, H. M. Weng, D. Prabhakaran, S.-K. Mo, Z. X. Shen, Z. Fang, X. Dai, Z. Hussain, Y. L. Chen, Science **343**, 864 (2014).

[278] M. Neupane, S.-Y. Xu, R. Sankar, N. Alidoust, G. Bian, C. Liu, I. Belopolski, T.-R. Chang, H.-T. Jeng, H. Lin, A. Bansil, F. Chou and M. Z. Hasan, Nature Commun. **5**, 3786 (2014).

[279] B. Buttner, C. X. Liu, G. Tkachov, E. G. Novik, C. Brne, H. Buhmann, E. M. Hankiewicz, P. Recher, B. Trauzettel, S. C. Zhang and L. W. Molenkamp, Nature Physics **7**, 418 (2011).

[280] M. Orlita, D. M. Basko, M. S. Zholudev, F. Teppe, W. Knap, V. I. Gavrilenko, N. N. Mikhailov, S. A. Dvoretskii, P. Neugebauer, C. Faugeras, A-L. Barra, G. Martinez and M. Potemski, Nature Physics **10**, 233 (2014).

[281] C. Nayak, S. H. Simon, A. Stern, M. Freedman, S. Das Sarma, Rev. Mod. Phys. **80**, 1083 (2008).